TAMPEREEN TEKNILLINEN YLIOPISTO
TAMPERE UNIVERSITY OF TECHNOLOGY

Antti Aronen

Modelling of Deformations and Stresses in Glass Tempering

Julkaisu 1036 • Publication 1036

Tampere 2012

Tampereen teknillinen yliopisto. Julkaisu 1036
Tampere University of Technology. Publication 1036

Antti Aronen

Modelling of Deformations and Stresses in Glass Tempering

Thesis for the degree of Doctor of Science in Technology to be presented with due permission for public examination and criticism in Konetalo Building, Auditorium K1702, at Tampere University of Technology, on the 13th of April 2012, at 12 noon.

Tampereen teknillinen yliopisto - Tampere University of Technology
Tampere 2012

ISBN 978-952-15-2799-9 (printed)
ISBN 978-952-15-2816-3 (PDF)
ISSN 1459-2045

ABSTRACT

Glass tempering is a heat treatment process which increases the strength of plate glass. In the past the process has been developed mainly on the basis of experimental results, but numerical modelling has now improved the ways of studying the process. The problems are most common with thin glass. A thin glass sheet requires high temperatures and rapid heat transfer to produce a good quality product. Furthermore the traditional support arrangements have to be modified. This thesis considers the most common quality faults and presents the reasons for their occurrence.

With thinner glass more effective heat transfer than is currently available is required to temper the glass. The increased heat transfer coefficient changes the mechanical behaviour so that a higher glass temperature is needed. However, the temperature increase makes the glass less viscous before cooling and the lower viscosity increases deformations.

The influences of temperature, heat transfer coefficient and support arrangements for glass plates have been investigated in this thesis using numerical methods. In the numerical modelling state-of-the-art models are presented and used. The cost effective one-dimensional dedicated program and a more general, three-dimensional commercial FEM program, are used in the simulations. The simulations explain and give more detailed information about the behaviour of glass.

The deformations are dependent on several parameters and the entire thermal and mechanical history has a bearing on the results. The results shown in this thesis can be used to design a new support system for a tempering furnace.

In the glass market the use of coated glass is increasing. The coating changes the thermal and mechanical behaviour of glass and the effect of coating on the glass behaviour has been demonstrated. The tempering of coated glass is more challenging than that of pure glass.

Although, the cases considered deal with the tempering process, the results can also be utilized in glass annealing.

PREFACE

This thesis was written while I was working as a teaching associate at Tampere University of Technology in the Department of Energy and Process Engineering from 2006 to 2010 and as a researcher in the same department in 2011. I would first, like to express my sincere thanks to my supervisor, Professor Reijo Karvinen, for his guidance and valuable advice throughout the research process. Additionally, I wish to thank all my colleagues at the Department of Energy and Process Engineering for a very inspiring working atmosphere. In particular, I would like to thank Dr. Markus Honkanen, Mr. Jarmo Ruusila and Mr. Matti Savela for sharing with me their expertise in the field of measurement.

Glaston Finland Oy is gratefully acknowledged for providing financial support during the work. I am also indebted to Mr. Mikko Rantala and Mr. Tarmo Pesonen for introducing me to the finer points of the glass tempering process. I would also like to acknowledge the Graduate School of Concurrent Mechanical Engineering and Professor Erno Keskinen for the financial support which enabled me to complete the thesis.

I also wish to express my thanks to my reviewers, Prof. Jens Schneider and Prof. Reijo Kouhia, for their excellent comments and suggestions.

Finally, I wish to thank my family and relatives for their support and encouragement throughout the ups and downs of this research. I also extend my thanks to all my friends who shared their time with me during the recent years.

Tampere, March 2012

Antti Aronen

NOMECLATURE

Latin letter symbols

$a(\Delta\lambda)$	Mean absorption coefficient	[1/m]
a	Roller-to-roller distance	[m]
b	Thickness	[m]
C	Weight coefficient of Prony Series for structural relaxation	
c	Thickness of coating film	[m]
c_p	Specific heat	[J/kgK]
E	Young's modulus	[N/m^2]
e	Deviatoric strain	
F_b	Fraction of radiative energy of black body spectrum	
f_b	Bending strength	[MPa]
G	Shear modulus, $G = E/2(1+\nu)$	[GPa]
g	Gravitional acceleration, 9.81	[m/s^2]
H	Activation energy	[J/mol]
h	Convective heat transfer coefficient	[W/m^{2}K]
I	Moment of inertia	[m^4]
K	Bulk modulus, $K = E/3(1-2\nu)$	[GPa]
k	Thermal conductivity	[W/mK]
L	Length	[m]
M	Moment	[Nm]
N	Normal force	[N]
Nn	Number of nodes	
q	Heat flux	[W/m^2]
q_{cr}	Cooling rate, $\partial T/\partial t$	[°C/s]
R	Universal gas constant, 8.314	[J/molK]
S	Radiative heat source	[W/m^3]
s	Deviatoric stress	[MPa]
T	Temperature	[°C or K]
T_f	Fictive temperature	[°C or K]

t	Time	[s]
u,v,w	Displacements	[m]
V	Glass velocity	[m/s]
$\dot{w}$	Tip velocity	[m/s]
$\dot{w}'$	Modified tip velocity	[1/s]
W	Width	[m]
w	Weight coefficient of Prony Series for stress relaxation	
x	Ratio of structural and glassy activation energy	
x,y,z	Coordinates	[m]

Greek letter symbols

α_m	Mean propagation angle	[°]
α	Expansion coefficient	[1/K]
β	Rotation	
δ_{ij}	Kronecker's delta	
ε	Strain	
$\bar{\varepsilon}$	Volumetric strain	
η	Viscosity	[Pa·s]
κ	Curvature	[1/m]
λ	Wave length	[m]
λ	Relaxation time for structural relaxation	[s]
ν	Poisson ratio	
ρ	Density	[kg/m^3]
ρ_m	Mean reflectivity	
σ	Stefan-Boltzmann constant, $5.67 \cdot 10^{-8}$	[W/m^{2}K^4]
σ	Stress	[MPa]
$\bar{\sigma}$	Volumetric stress	[MPa]
τ	Relaxation time for stress	[s]
ξ	Reduced time	[s]
ϕ'''	Heat generation	[W/m^3]
ϕ	Shape factor	

Subscripts

c	Creeping
g	Glass
i	Index
l	Liquid
m	Mean
mid	Mid-plane
n	Node
r	Reference value
ref	Reference state
s	Structural
s	Solid
t	Temperature
$surf$	Surface
u	Uniaxial
0	Initial state
∞	Infinity
∞	Environment

Superscripts

D	Delayed
E	Elastic
m	Mechanical
th	Thermal
V	Viscous
ve	Viscoelastic

Abbreviation

FEM	Finite element method
SLS	Soda-lime-silica

TABLE OF CONTENTS

1. INTRODUCTION

1.1. Background and motivation of research

Commercial annealed soda-lime-silica glass is weak under tension but strong under compression. The theoretical strength of glass is over 10 000 MPa (Le Bourhis 2008). The weakness under tension is caused by the small surface flaws which tend to grow under the effect of the tensile stress. Glass is a brittle material at room temperature and deformations are elastic until fracture (Le Bourhis 2008). The strength of glass can be improved in three ways: by removing the surface flaws, by avoiding the formation of the flaws on the surface or by making the flaws inoperative. The last method has been found to be the most effective, which means that a compressive stress has to be created in the surface (Bartholomew & Garfinkel 1980). With a compressive stress layer in the surface, glass can be strengthened. The strengthening can be performed in two ways, either by thermal or chemical strengthening. In Fig. 1.1 the typical stress profiles for thermally and chemically strengthened glasses are presented.

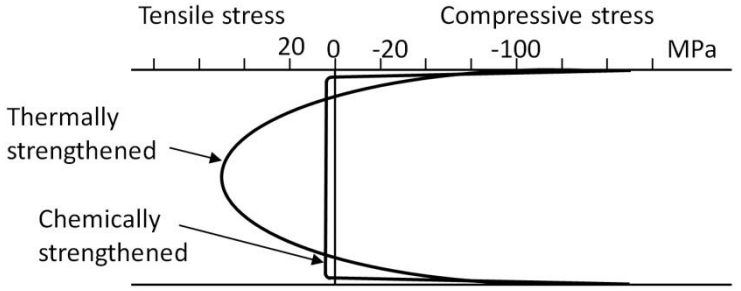

Figure 1.1. Stress profile of tempered and chemically strengthened glass.

In thermal strengthening, the compression in the surface can be reached with the help of the heat treatment and at the same time tensile stress is created in the mid-plane. Thermal strengthening typically results in two stress levels: tempered glass with a surface compressive stress of more than 80-100 MPa and heat strengthened glass with a surface compressive stress of 45-65 MPa. The surface compression is not the only feature of interest in tempering. Another feature, almost as important, is the mid-plane tension which gives rise to better fragmentation in the case of breakage. Fragmentation of annealed and tempered glasses after breaking with a sharp point is shown in Fig. 1.2. In Fig. 1.2a the thickness of the annealed glass is 3.3 mm and in Fig. 1.2b the thickness of the tempered glass is 2.8 mm.

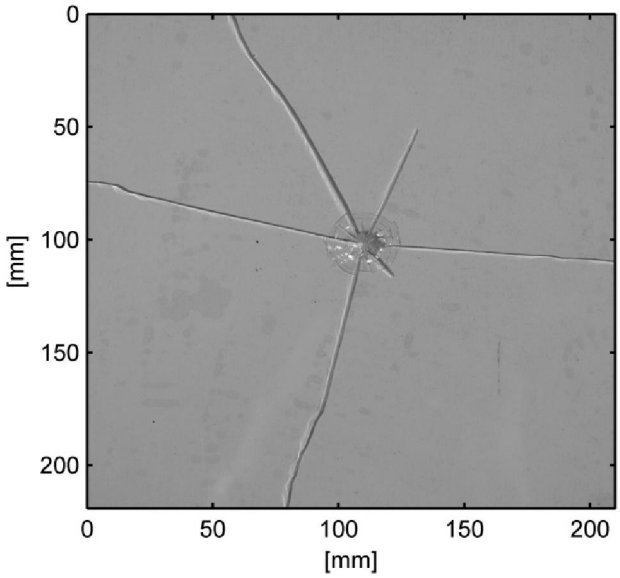

a)

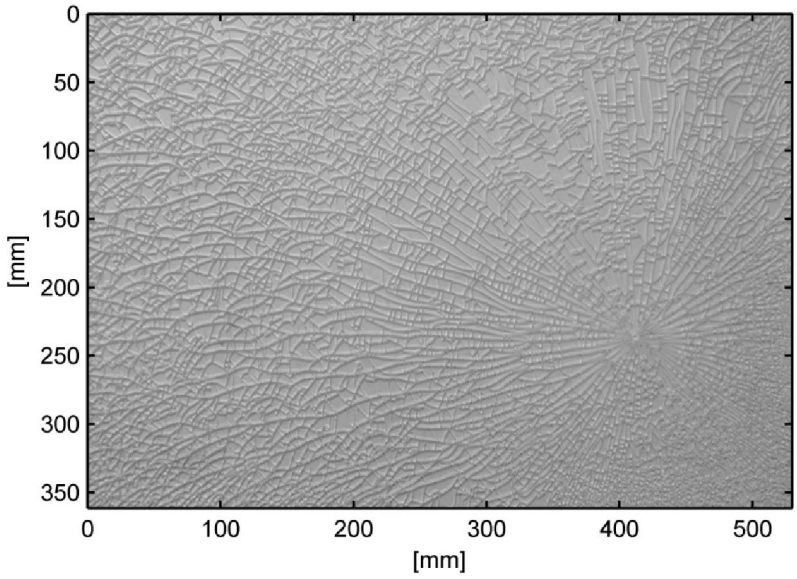

b)

Figure 1.2. Fragmentation of (a) annealed and (b) tempered glass after breaking with a sharp point.

In chemical strengthening, with the help of the ion exchange, a high compressive stress is created in the surface but only a small tensile stress forms in the centre because of the small thickness of the compression layer.

The thermal strengthening or tempering is based on the heat treatment of the glass. In the process, glass is heated above the transition temperature and then cooled rapidly (quenched) by air jets to below the transition temperature, which is approximately 550 °C for a soda-lime-silica glass. Tempering results depend on the temperature level before cooling and heat transfer during cooling. During the process the glass moves on rollers.

Tempered glass is a very common building material. Many façades or windows are made from tempered glass because of its good strength. Usually tempered glass is located in a visible place and customers want tempered glass to have good visual properties. The strength is usually the most important requirement but the visual aspects are becoming increasingly important. There can be different kinds of visual faults in glass, as shown in Figs. 1.3-1.7: roller waving, longitudinal or cross patterns, distorted reflection or transparency or white hazes (Henriksen & Leosson 2009). Visual faults in Figs. 1.3-1.6 are caused by too high a process temperature and the fault in Fig. 1.7 is caused by uneven heat transfer.

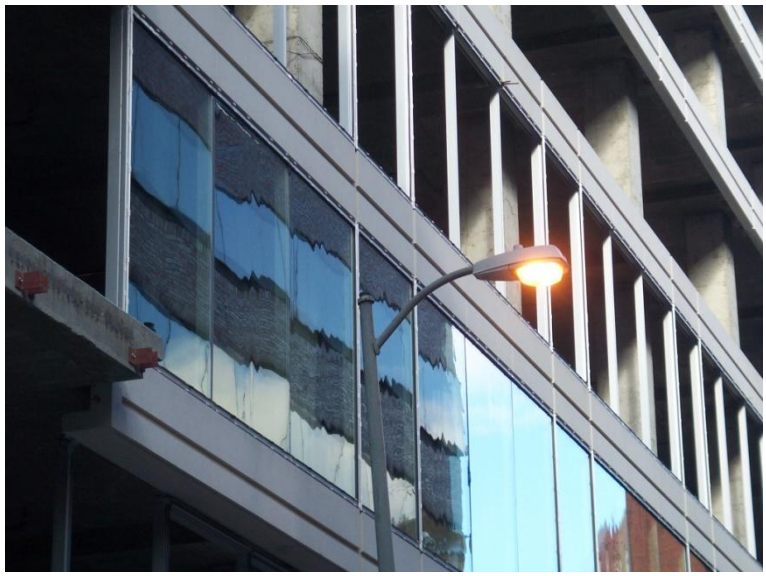

Figure 1.3. Roller waves (Henriksen & Leosson 2009).

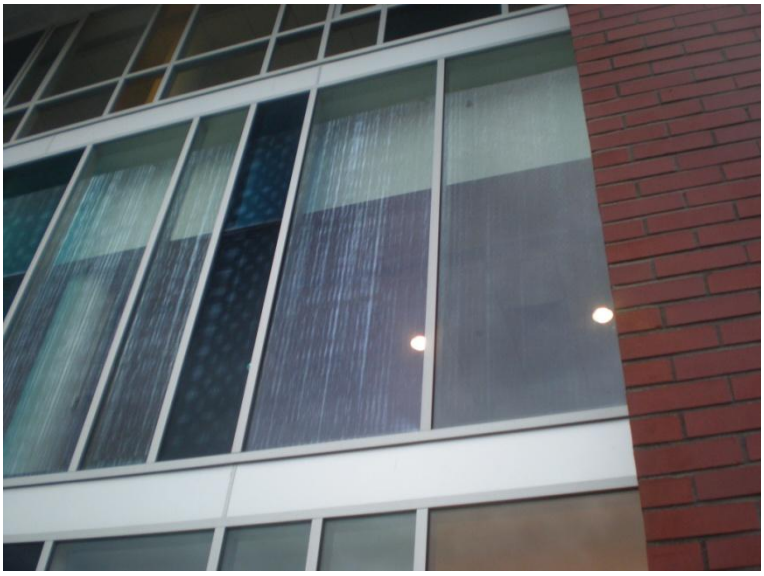

Figure 1.4. Longitudinal patterns (Henriksen & Leosson 2009).

Figure 1.5. Cross patterns (Henriksen & Leosson 2009).

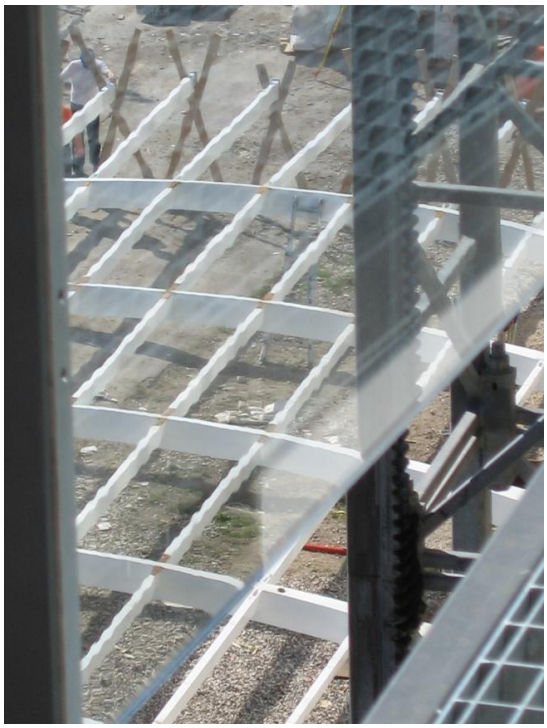

Figure 1.6. Distorted reflection or transparency (Henriksen & Leosson 2009).

Figure 1.7. White haze (Henriksen & Leosson 2009).

The tempering process needs to produce good quality. Standards exist under which strength and distortion are determined (ASTM C1048-97b 2007, EN12150-1 2000), but customers can have also their own specific requirements. In recent years, the demand for thin glass has increased and the market now requires even thinner glasses. The difficulties of making good quality products increase with thinner glass.

Similar phenomena to those found in the tempering process are met with in annealing process. In the annealing process, glass is cooled slowly through the transition range to minimise the residual stresses. Processes like cutting and drilling of holes are then possible. In general, annealing is part of the float process, but annealing can also be used in some heat treatment processes when low residual stress is required, as, for example, in coating processes.

To improve quality, the major obstacles to good quality must be identified. The identification can be achieved by investigating the entire process. With modelling we can easily study the phenomena without expensive experimental measuring devices or glass fragmentation tests. Measuring devices, which utilize photoelasticity, have been developed for stress measurements. Even though modelling is the way to study the formation of stresses and the means by which measuring devices are developed, currently the only reliable way to test quality is the fragmentation test.

Tempering is an old process as is the history of mathematical modelling of a tempering phenomenon. The history of model development is reviewed by Gardon (1980), Guillemet (1990) and Narayanaswamy (2001). The first patent relating to the tempering process was granted in 1877 (Siemens 1877). Since the process was first invented it took over four decades until the first mathematical expressions about stress forming were presented in 1920 by Adams and Williamson. Their theory about stress production is based on cooling at a uniform rate. When the cooling rate is constant the temperature gradient is also constant and new strains are not produced. This model also contained the assumption that the whole glass plate solidifies at the same time. They stated the rule as follows: “the permanent stresses which are set up in glass are of opposite sign and equal to the stresses released at the beginning of cooling”. The equation by Adams and Williamson worked well for annealing since the cooling rate was kept constant in the annealing furnace.

The next development step was the Instant Freezing Model developed by Bartenev (1948). The model assumes that the change between viscous and elastic state takes place instantaneously at the transition temperature. Moreover, the model assumes that the freezing takes place a relatively long time after the beginning of cooling and the maximum temperature gradient is produced before solidification. The model was later modified by Indenbom (1954).

The next significant step in tempering modelling was to improve the material model for glass. Until this time it had been thought that a material is either elastic or viscous. In the 1960s Kurkjian (1963) proved that stabilized glass is a linear viscoelastic material. He also showed that the relaxation curves at different temperatures can be derived by a

change in the time scale. This is called thermorheological simplicity. Lee, Rogers and Woo (1965) proposed a tempering model using the more realistic viscoelastic properties of glass which permitted a continuous increase in viscosity with decreasing temperature.

All three models above take into account the change from elastic to viscous properties. In 1978 Narayanaswamy introduced a theory concerning volume relaxation. The theory is based on the idea by Tool (1946) about the fictive temperature. The volume relaxation is the time dependent volume change which follows the instantaneous volume change caused by temperature change. At high temperatures the volume of glass continues to increase causing an additional strain equal to twice the instantaneous thermal strain. This concept is referred to as structural relaxation.

Recently, many researchers have used modelling to calculate residual stresses in tempered glass. For example, there are papers dealing with the stress profiles through the thickness of the glass (Gardon 1998, Kong *et al.* 2007). Usually these are calculated using a one-dimensional model. There are also papers in which the stress profile around a hole or an edge is studied (Daudeville & Carré 1998, Schneider 2004, Maniatis 2005 and Nielsen *et al.* 2010a). In these cases two- or three-dimensional treatment, using finite element (FEM) codes, are needed.

In the literature few authors have written about visual quality. Most of the articles which deal with visual quality discuss the visual faults and give the reasons for them (Henriksen & Leosson 2009, Abbott & Madocks 2001). The effects of temperature, heat transfer coefficient and the support system have not been widely studied.

For the modelling, information concerning heat transfer is needed. Because glass is a semi-transparent material, the impact of radiation is more complicated than with opaque glass when all the radiation is absorbed on the surface. The theory of radiation in glass has been studied by Gardon (1958) and Field & Viskanta (1990). The conduction and convection of heat in glass are similar to that in other materials.

Forced convection can be created with impinging air jets. The behaviour of air jets is presented in many papers. The heat transfer characteristics of a nozzle are reviewed by Zuckerman & Lior (2006), the behaviour of nozzles is also studied by Huber and Viskanta (1994) and the mean heat transfer of an array of round nozzles is studied by Holger (1977). In the tempering process glass plates can move with a velocity of over 0.5 m/s. Thus, the heat transfer coefficient can be considered to be approximately uniform over the whole plate. The effect of local variation of heat transfer coefficients on residual stresses is also studied in the thesis.

The measuring of residual stresses is complicated because the only destructive measuring method for tempered glass is the fragmentation test. However because glass is a transparent material, non-destructive measuring methods are possible. There are optical methods based on photoelasticity. In these measurements the birefringence of light waves depends on the density of material.

In the 1960s Gardon (1965) made measurements of glass temperatures and stress profiles, and these results are still valid. In these results the effect of temperature and heat transfer on the transient and residual stresses are shown. Some new results based on the earlier work were also presented in the 1980s by Gardon (1980).

1.2. Objectives and outline of thesis

The main objective of this thesis is to present a state-of-the-art model for a tempering process as well as results from investigation of the effects of different phenomena on the process. The main component of the thesis is the presentation of the biggest problems in 2 mm or thinner glass tempering and together with the theoretical reasons for different kinds of visual defects.

The first chapter presents background information about the quality of tempered glass. In addition, mathematical models of the tempering process are reviewed. Chapter 2 gives more information about soda-lime-silica glass which is the most common material for tempered glass. In the same chapter the tempering and chemical strengthening processes are introduced.

Chapter 3 reviews the theory of heat transfer and mechanical behaviour of glass and presents the state-of-the-art model of the tempering process. In Chapter 4, the equations needed for the numerical calculations in a one-dimensional case are presented. With that model the stress profile through the thickness can be calculated at a distance from edges. The curving and bending of glass can also be calculated when the loading is known.

Chapters 5 and 6 concentrate on the simulation cases for the one-dimensional model. In Chapter 5 the results for through the thickness stress profile calculations are presented and compared with measurements in the literature. In Chapter 6 the results are shown for glass bending due to its own weight. In Chapter 7 the commercial FEM program, Ansys® 13.0 Academic Research, has been used to study the effect of time and locally dependent heat transfer and glass support on stresses and deformations in the glass. The theory used in the Ansys code is the same as that in the model of Chapter 3.

The calculation methods, and the results they give, are further discussed in Chapter 8 as conclusions.

2. GLASS PROPERTIES AND STRENGTHENING PROCESSES

2.1. Glass properties

The term “glass” is used for many materials. Usually “glass” is considered to be a transparent solid, but “glass” can also have other appearances. Glass is an amorphous solid completely lacking in long range, periodic atomic structures, and having a region of time-dependent glass transformation behaviour (Shelby 2005). Glass which is used in windows and buildings is called soda-lime-silica (SLS) glass. In the thesis the term “glass” is used to refer to SLS glass. The typical composition of commercial SLS glass is given in Table 2.1.

Table 2.1. Chemical composition of soda-lime-silica glass (EN 572-1, 2004).

Chemical compound		Weight-%
Silicon dioxide	SiO_2	69-74
Calcium oxide	CaO	5-14
Sodium oxide	Na_2O	10-16
Magnesium oxide	MgO	0-6
Aluminium oxide	Al_2O_3	0-3
Others		0-5

Glass is considered to be a time-independent, perfectly linear, isotropic elastic solid at room temperature. The mechanical and thermal properties are composition dependent. Typical values of different properties at room temperature are given in Table 2.2.

Table 2.2. General characteristic values of glass (EN 572-1, 2004).

Property	Symbol	Value	Unit
Density	ρ	2500	kg/m^3
Young’s modulus	E	70	GPa
Poisson’s ratio	ν	0.2	
Bending strength	f_b	45	MPa
Thermal expansion coefficient	α	$9 \cdot 10^{-6}$	1/K
Specific heat	c_p	720	J/kgK
Thermal conductivity	k	1	W/mK
Emissivity	ε	0.837	

The tensile strength of annealed glass varies from 30 MPa to 100 MPa depending on the quality of the surface and the edges (Le Bourhis 2008, Nielsen 2009, Maniatis 2005).

In the tempering process the glass temperature is raised over 600 °C. At high temperatures glass viscosity decreases and it can no longer be considered as an elastic solid but it is now a viscoelastic material. With a viscoelastic model both the viscous and

elastic properties can be taken into account. The change from a glassy state to a liquid state affects many material properties and the behaviour of material.

In the tempering process, knowing the material properties at high temperature is important. Properties are presented in many papers (Carré & Daudeville 1996, 1999, Daudeville *et al.* 2002, Scherer & Rekhson 1982, Kurkjian 1963, Gardon 1958, Field & Viskanta 1990). There are differences between the various material properties that have been presented in the literature. Some differences are caused by chemical differences between the glasses measured. Properties used in this thesis are presented in Appendix A.

2.2. Tempering process

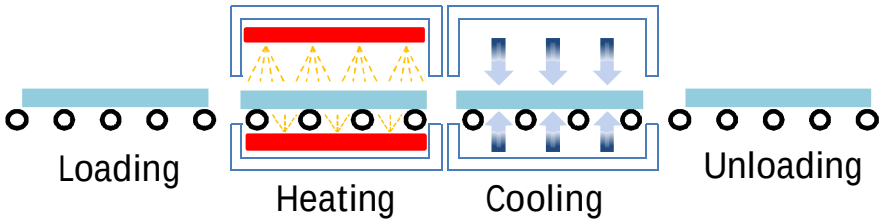

Figure 2.1. Sketch of tempering process.

Thermal strengthening or tempering is based on heat treatment of the glass. A sketch of the tempering process is presented in Fig. 2.1. In the process, glass is first heated to above the transition temperature in the furnace. At temperatures above the transition temperature glass is viscous enough to create viscous strains instead of elastic strains. Heat transfer during heating is mainly by radiation. Forced convection has to be used to balance the temperature field in glass, especially with so-called Low-E (low emissivity) glasses where a surface is coated. After heating, the temperature through the sheet is uniform and small stresses are dependent only on the support structure. Some deformation can be formed due to the creeping of glass.

After heating, the glass goes into the cooling section where it is cooled rapidly (quenched) to below the transition temperature with forced convection by air jets. At the beginning of cooling, the surface temperature drops faster than in the mid-plane and the surface tries to shrink more than the mid-plane. In the case of symmetric cooling, the total strain should be uniform over the thickness and the differences due to the thermal strain are equalized by elastic and viscous strains, depending on the temperature. Due to the lower temperature on the surface, tension is formed on the surface and compression in the mid-plane. However, due to viscosity, the stresses do not rise to the same level as when the behaviour is caused by pure elasticity.

Later, during cooling, the glass temperature profile becomes flat and the mid-plane shrinks more than the surface so that compression is created on the surface and tension in the mid-plane, as shown in Fig. 2.2.

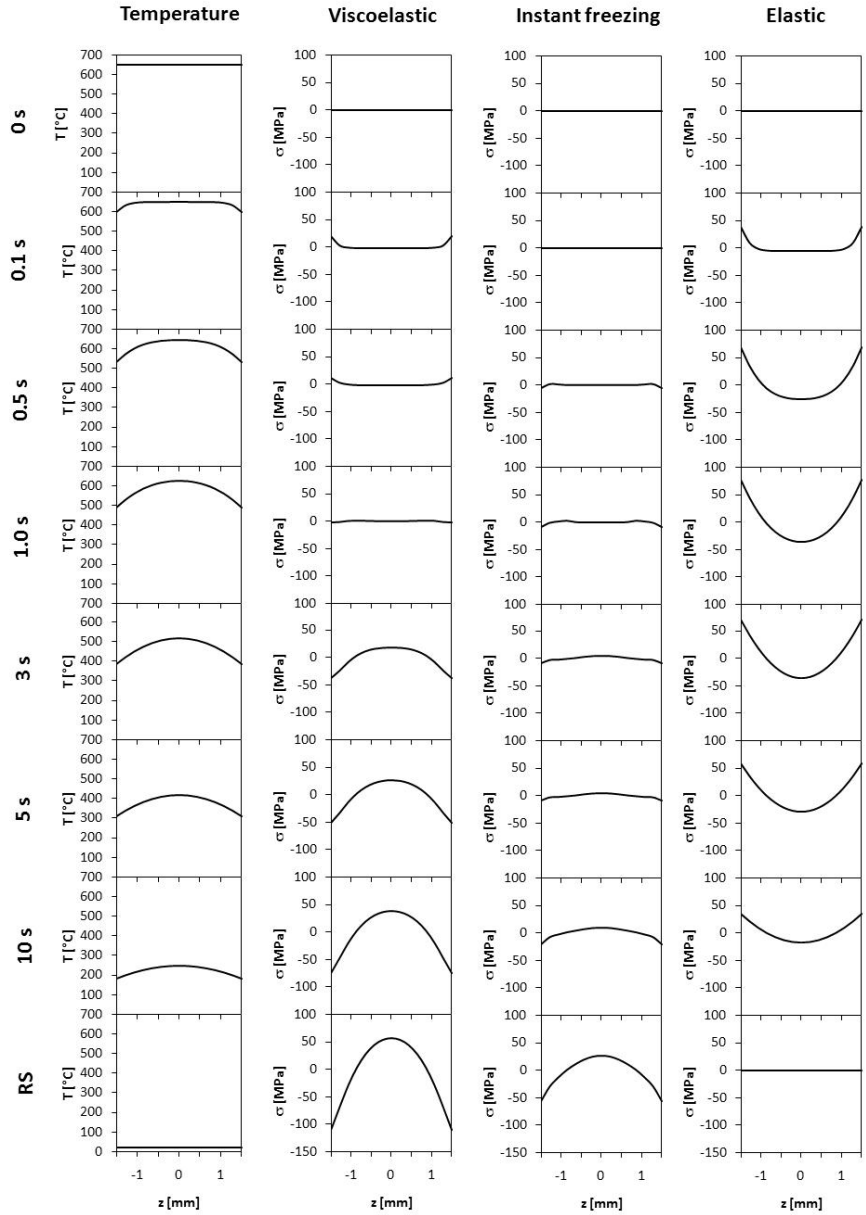

Figure 2.2. Temperature and stress distributions during cooling with three different mechanical models. Glass thickness is 3 mm, T_0 is 650 °C and h is 600 W/m^{2}K.

The temperature level before cooling and heat transfer during cooling affect the tempering. During the process, glass is moved on rollers to avoid local heat transfer variation and to make the support more even.

Residual stresses are created during the cooling. The temperature field dominates the tempering process and, due to the viscoelastic behaviour, residual stresses are the result.

Figure 2.2 presents the stress profiles with three different thermo-mechanical models. The results are calculated with a one-dimensional program, which is based on the theory presented in the Chapter 3.

In the elastic case, no residual stresses are created. With instant freezing (freezing temperature is 590 °C) but without structural relaxation, stresses stay lower than with the viscoelastic model with structural relaxation. The results from the viscoelastic model are used for glass.

2.3. Chemical strengthening

The purpose of chemical strengthening is to create a compression layer at the surface with the help of ion exchange in either of two ways. The first method is to replace, at a temperature above T_g (glass transition temperature is about 550 °C), ions in the surface having a larger thermal expansion coefficient with those having a smaller thermal expansion coefficient. The sodium Na^+ ions of the surface are replaced by Li^+ ions. In this case the expansion coefficient at the surface will become smaller and at the cooling stage the centre of the glass will shrink more than at the surface, creating compression in the surface.

Another way is to replace smaller ions in the surface with larger ones at a temperature below T_g. The usual method is the replacement of smaller sodium Na^+ ions with larger potassium K^+ ions. In this case, the surface will try to grow but the rigid glass network does not permit the growth which might have been caused by the bigger ions. Instead, compression is created in the surface layer.

In the literature the effect of different ion exchange methods, temperatures and times on the stresses in the surface has been comprehensively presented in 1980 by Bartholomew and Garfinkel as well as more recently by Karlsson *et al.* (2010). The compressive stress layer which forms at the surface is very thin (usually < 100 μm) in both cases. With the chemical strengthening, a strength of more than 150 MPa can be easily reached.

In Fig 1.1 the stress profiles of thermally and chemically strengthened glasses are shown. It can be seen that in thermally strengthened glass, the tensile stress in the mid-plane is much higher than in chemically strengthened glass. Because of a high tensile stress in the mid-plane, glass breaks into small harmless fragments if broken. Usually the tensile stress of chemically strengthened glass is small and fragmentation does not occur during breakage.

Both strengthening methods (thermal and chemical) have their advantages and disadvantages. Table 2.3 presents the essential differences between thermally and chemically treated glasses according to Karlsson *et al.* (2010). The stress profiles are significantly different such that cutting or drilling, for example, of thermally strengthened glass is not possible. With a chemical process, even 0.5 mm thick glass plate can be strengthened, whereas with thermal strengthening the thickness must be greater than 2 mm. Thermally strengthened glass is used in architectural and in

automobile applications. Chemically strengthened glass is much less used, mainly due to its high cost. The high cost of chemical strengthened glass is partly due to the long treatment time.

Table 2.3 shows that material properties must also take into account both strengthening methods. In the tempering process a relatively high thermal expansion coefficient is needed whereas the chemical strengthening method depends on the glass composition. Chemical strengthening is more applicable for unusual shapes and abraded samples. In the tempering process spontaneous breakage is possible due to the tensile stresses during the process. In the tempering process visual faults are common, especially with thin glass.

Table 2.3. Comparison of thermal and chemical strengthening (Karlsson *et al.* 2010).

	Thermal strengthening	Chemical strengthening (low temperature process)
Maximum strength	175 – 400 MPa	100 – 1000 MPa
Stress distribution profile	Parabolic	Flatter, more square
Surface compression	Relatively thick	Thin surface compression unless treatment time lengthened
Mechanical treatment after strengthening	No cutting or drilling is possible	Might be cut or drilled or ground depending on the internal tension
Price	Less expensive	More expensive
Glass thermal expansion	Relative high values required	Not important
Optical distortion	Heating and chilling must be carefully controlled to avoid distortion	No significant distortion of ware
Spontaneous breakage	Yes	No
Time of treatment	Short time required (minutes)	Long time required (hours)
Sample thickness	Minimum 2 mm	0.5 mm to 15 mm
Shape	Not applicable to shapes where all surfaces are not freely accessible to chilling medium	Applicable to unusual shapes
Glass composition	Applicable to most glasses	Special glass compositions
Strengthening of abraded samples	No	Yes

3. THEORETICAL BASIS OF MECHANICAL TEMPERING

Glass tempering is a heat treatment process. The temperature change as a function of time governs the process and affects thermal strains and mechanical behaviour. Only heat transfer and glass support affect the tempering process. In addition, the mechanical behaviour depends on the material properties.

In this chapter the theory needed for temperature and mechanical calculations is given. The mechanics proceed from thermoelasticity to thermoviscoelasticity and other glass behaviour characteristics.

The theory is concentrated on the plate, the length and the width of which are much bigger than the thickness. In addition, the temperature field is considered to vary only in the thickness direction and edge behaviour is ignored. The theory of heat transfer is covered in many books dealing with the basic concepts of conduction, convection and radiation (Mills 1999, Bejan 1993). Specific knowledge concerning radiative heat transfer is presented, for instance, in Siegel & Howell (2001) and Modest (1993).

Three-dimensional equations of mechanical behaviour are presented. In the case of a glass plate, the behaviour can be simplified to the plane stress where the temperature only changes in the thickness direction. The mechanical behaviour is based on thermal stresses (Boley & Weiner 1997, Noda *et al.* 2003) and viscoelasticity (Flügge 1975, Christensen 1982). The theory of structural relaxation presented here follows the work by Scherer (1986).

3.1. Heat transfer

In a tempering process, during the heating heat transfer is controlled by radiation and convection from the furnace to the glass and by radiation and conduction in the glass. Radiation in glass is complex because it is a semi-transparent material in which absorption, reflection and transmission depend on the wavelength of the radiation. Forced convection has to be used in heating to balance the temperature field in glass, especially with so-called Low-E (low emissivity) glasses where a surface is coated. Forced convection must be used in cooling to increase convection and balance heat transfer.

Heat transfer during the glass tempering process is time-dependent. The calculation of heat transfer is based on the 1D energy equation in the z direction

$$\rho c_p \frac{\partial T}{\partial t} = \frac{\partial}{\partial z}\left(k \frac{\partial T}{\partial z}\right) + S \tag{3.1}$$

where ρ is the density, c_p is the specific heat, t is time, T is temperature, k is the thermal conductivity and S is the heat source term for radiation inside the glass.

In order to solve Eq. (3.1) boundary conditions in the glass surface have to be fixed. For instance, in the case where contact heat transfer is combined with convection, the boundary condition can be presented by using the effective heat transfer coefficient *h* on the lower surface in Fig. 3.1. The heat flux *q* is

$$q = -k\left(\frac{\partial T(-b/2\,,t)}{\partial z}\right) = h(T(-b/2\,,t) - T_\infty) \tag{3.2}$$

where b is the thickness of the plate, T_∞ is the ambient temperature and h is the heat transfer coefficient, which includes convection and contact heat transfer. A similar type of equation is also needed in the upper surface.

In addition to convection, radiation, to and from the surface, must be taken into account. The convective heat transfer coefficient h depends on many parameters, such as the fluid, the velocity, the temperature and the nozzle-distance. The main issue is not how convective heat transfer is evaluated. The convective heat transfer coefficient is assumed to be known.

The source term for radiation in a glass is dependent on the wavelength. In our case the absorption in glass in Eq. (3.1) is approximated as (Rantala & Karvinen 2001)

$$S \approx \sum_{i=1,j=2}^{i=k,j=k+1} \left\{ \begin{array}{c} \left[F_b(\lambda_i,\lambda_j,T_\infty)\sigma T_{\infty u}^4 - F_b(\lambda_i,\lambda_j,T)\sigma T^4\right]\dfrac{(1-\rho_m)}{1-\dfrac{\rho_m \exp(-a(\Delta\lambda_i)b)}{\cos(\alpha_m)}} \\ \left[\exp\left(-\dfrac{a(\Delta\lambda_i)(b/2-z_1)}{\cos(\alpha_m)}\right) - \exp\left(-\dfrac{a(\Delta\lambda_i)(b/2-z_2)}{\cos(\alpha_m)}\right)\right] \\ +\left[F_b(\lambda_i,\lambda_j,T_\infty)\sigma T_{\infty d}^4 - F_b(\lambda_i,\lambda_j,T)\sigma T^4\right]\dfrac{(1-\rho_m)}{1-\dfrac{\rho_m \exp(-a(\Delta\lambda_i)b)}{\cos(\alpha_m)}} \\ \left[\exp\left(-\dfrac{a(\Delta\lambda_i)(b/2+z_2)}{\cos(\alpha_m)}\right) - \exp\left(-\dfrac{a(\Delta\lambda_i)(b/2+z_1)}{\cos(\alpha_m)}\right)\right] \end{array} \right\} \tag{3.3}$$

where $F_b(\lambda_i,\lambda_j,T)$ is the fraction of radiative energy of a black body between wavelengths λ_i and λ_j in the ambient temperature T_∞ and σT^4 is the blackbody emissive power. z_1 and z_2 are the coordinates of element surfaces. In Fig. 3.1 the reflection and transmission of incident radiation in the glass are presented. In the case of radiation for temperature units [K] has to be used.

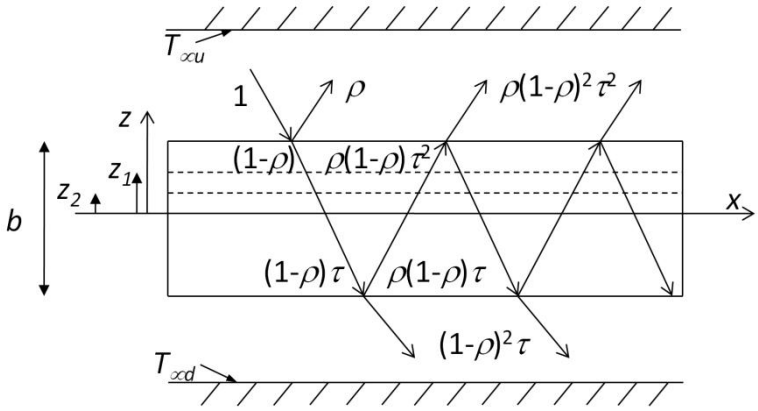

Figure 3.1. Reflection and transmission of incident radiation.

Wavelengths have been divided into three sections. Each section has its own absorption coefficient. Values are presented in Appendix A (Table A.3). For those absorption coefficients the mean reflectivity ρ_m is 0.04 and the mean propagation angle α_m is 0°. The fraction of radiative energy of a black body between wavelengths λ_i and λ_j can be calculated from equation (Siegel & Howell 2001)

$$F_b(\lambda_i, \lambda_j, \mathrm{T}) = F_{0\to\lambda_j T} - F_{0\to\lambda_i T} \tag{3.4}$$

where

$$F_{0\to\lambda T} = \frac{15}{\pi^4}\sum_{m=1}^{\infty}\frac{e^{-mv}}{m^4}\{[(mv+3)mv+6]mv+6\} \tag{3.5}$$

In Eq. (3.5) v is dependent on wave length λ and temperature T

$$v = \frac{C_2}{\lambda T} \tag{3.6}$$

and C_2 is 1.4388 cmK. In the calculations, the four first terms of Eq. (3.5) are used.

In heat transfer calculations it should be noted that the specific heat is time- and temperature-dependent. The specific heat c_p in the transition range is the combination of the specific heat of the equilibrium liquid $c_{p,l}$ and the specific heat in a glassy state $c_{p,g}$

$$\int_{T_0}^{T} c_p(T')dT' = \int_{T_0}^{T_f} c_{p,l}(T')dT' + \int_{T_f}^{T} c_{p,g}(T')dT' \tag{3.7}$$

The specific heat in a glassy state is linearly temperature dependent and constant in the equilibrium liquid. The fictive temperature T_f is dependent on structural relaxation, which is presented in Section 3.2.3 below. The thermal conductivity k in Eq. (3.1) is linearly dependent on temperature. For temperature dependent material properties [K] or [°C] are used for units of temperature depending on the correlation.

3.2. Mechanical behaviour of glass

A three-dimensional theory of glass mechanical behaviour is presented. The three-dimensional equations are easily simplified to show plane stress or plane strain, for example. In the case of glass, the behaviour obeys the plane stress equations except near the edges.

3.2.1. Elastic behaviour

When the temperature distribution is known, the stress and deformation field can be calculated. At low temperatures the glass behaviour is elastic. The thermoelastic stress-strain relation is presented with constitutive equation (3.8) (Boley & Weiner 1997). The strain ε_{ij} and stress σ_{ij} can be divided into volumetric ($\bar{\varepsilon}$, $\bar{\sigma}$) and deviatoric (e_{ij}, s_{ij}) parts (Carré & Daudeville 1999)

$$\sigma_{ij} = \delta_{ij}\frac{1}{3}\bar{\sigma} + s_{ij} = K(\bar{\varepsilon} - 3\varepsilon^{th})\delta_{ij} + 2Ge_{ij} \tag{3.8}$$

where K is the bulk modulus, G is the shear modulus, δ_{ij} is Kronecker's delta and

$$\bar{\sigma} = \sigma_{xx} + \sigma_{yy} + \sigma_{zz} \tag{3.9}$$

$$s_{ij} = \sigma_{ij} - \delta_{ij}\frac{1}{3}\bar{\sigma} \tag{3.10}$$

$$\bar{\varepsilon} = \varepsilon_{xx} + \varepsilon_{yy} + \varepsilon_{zz} \tag{3.11}$$

$$e_{ij} = \varepsilon_{ij} - \delta_{ij}\frac{1}{3}\bar{\varepsilon} \tag{3.12}$$

$$\varepsilon^{th} = \alpha(T - T_0) \tag{3.13}$$

In Eq. (3.13) α is the thermal expansion coefficient and T_0 is the initial or reference temperature.

The stress field can be calculated by using the compatibility equations expressed in terms of stress components (Boley & Weiner 1997) as

$$(1+\nu)\nabla^2\sigma_{ij} + \frac{\partial^2\bar{\sigma}}{\partial x_i \partial x_j} + \alpha E\left(\delta_{ij}\frac{1+\nu}{1-\nu}\nabla^2 T + \frac{\partial^2 T}{\partial x_i \partial x_j}\right) = 0 \tag{3.14}$$

where E is Young's modulus and ν is Poisson's ratio.

In the freely supported plane stress case, the stress components in the x and y directions are similar and other stress components are zero. In Fig. 3.2 the y direction is perpendicular to x-z-plane.

$$\sigma_{xx} = \sigma_{yy};\ \ \sigma_{zz} = \sigma_{xy} = \sigma_{yz} = \sigma_{zx} = 0 \tag{3.15}$$

The only remaining stress σ_{xx} must fulfil equations

$$\int_{-b/2}^{b/2} \sigma_{xx} dz = 0 \tag{3.16}$$

$$\int_{-b/2}^{b/2} \sigma_{xx} z dz = 0 \tag{3.17}$$

The stress distribution in a glass plate is obtained by solving the compatibility equation in the z direction

$$\sigma_{xx}(z) = \sigma_{yy}(z) = \frac{1}{1-\nu}\left(-\alpha E(T(z) - T_0) + \frac{1}{b}N_t + \frac{12z}{b^3}M_t\right) \tag{3.18}$$

where

$$N_t = \alpha E \int_{-b/2}^{b/2} (T(z) - T_0) dz \tag{3.19}$$

and

$$M_t = \alpha E \int_{-b/2}^{b/2} (T(z) - T_0) z dz \tag{3.20}$$

The Kirchhoff-Love hypothesis can be used for strain calculations. The plane initially perpendicular to the neutral plane of the plate also remains a plane after the deformation and is perpendicular to the deformed neutral plane (Noda *et al*. 2003)

$$\varepsilon_{xx}(x, y, z, t) = \varepsilon_{xx}^0(x, y, t) + \kappa_x(x, y, t) z \tag{3.21}$$

$$\kappa_x(x, y, t) = \frac{\partial \beta_x(x, y, t)}{\partial x} \tag{3.22}$$

where ε_{xx}^0 is the strain of mid-plane, κ_x is the curvature and β_x is the rotation of the reference surface about the y axis.

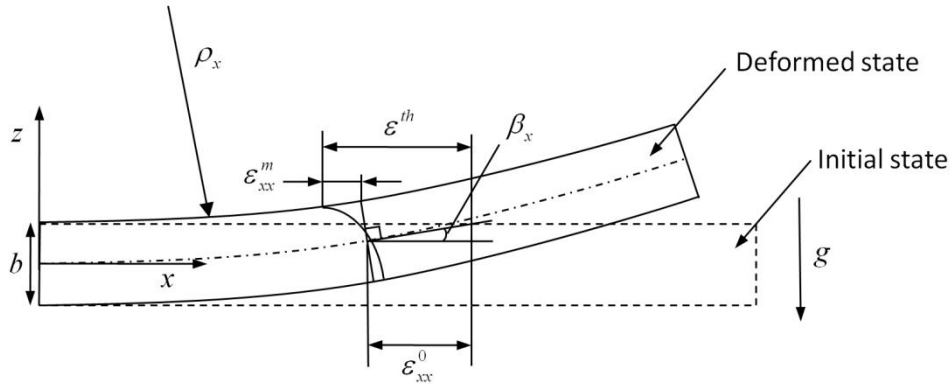

Figure 3.2. Strains in glass plate.

The deformations in the y direction are similar but in the z direction the curvature is neglected in the case of the plate. Figure 3.2 shows the strains and curvature in the x direction. ρ_x is the radius of curvature which is the inverse of curvature $1/\kappa_x$, ε^m_{xx} is the mechanical strain which causes the stresses.

3.2.2. Viscoelastic behaviour

At high temperatures, above the transition temperature, the effect of viscoelasticity must be taken into account. The viscoelasticity can be presented with the Maxwell model where the spring and the damper are in series.

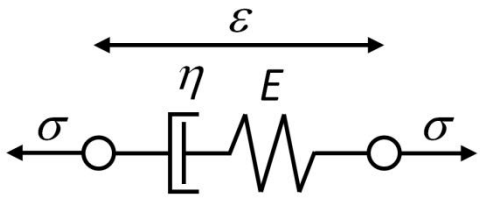

Figure 3.3. Maxwell model.

The constitutive equation for the Maxwell model in Fig. 3.3 is

$$\dot{\varepsilon} = \frac{\dot{\sigma}}{E} + \frac{\sigma}{\eta} \tag{3.23}$$

where η is the viscosity. The relation between the stress and strain is obtained from Eq. (3.23) by using Laplace-transform equations

$$\sigma = E\exp\left(-\frac{t}{\eta/E}\right)\varepsilon = E\exp\left(-\frac{t}{\tau_u}\right)\varepsilon \tag{3.24}$$

In this equation τ_u is the relaxation time in the uniaxial case.

However, in the three-dimensional case the stress-strain relation should be presented according to Eq. (3.8). Because the strain and temperature can change as a function of time, the whole time history has to be taken into account (Carré & Daudeville 1999). The stress-strain relation is presented with a hereditary integral (Flügge 1975), as

$$\sigma_{ij}(t) = \delta_{ij} \int_0^t K(t-t') \frac{\partial(\bar{\varepsilon} - 3\varepsilon^{th})}{\partial t'} dt' + 2 \int_0^t G(t-t') \frac{\partial(e_{ij})}{\partial t'} dt' \tag{3.25}$$

The bulk and shear relaxation moduli for the generalized Maxwell model can be presented with Prony's series by dividing the relaxation curve with weighting factors *w* and relaxation times τ

$$K(t) = K_\infty + (K_0 - K_\infty) \sum_{p=1}^{P} w_{2p} \exp\left(-\frac{t}{\tau_{2p}}\right) \tag{3.26}$$

$$G(t) = G_0 \sum_{q=1}^{Q} w_{1q} \exp\left(-\frac{t}{\tau_{1q}}\right) \tag{3.27}$$

where subscript 0 is the initial value and ∞ is the value at infinite time. In the weighting factors and relaxation times the subscript 1 is for the shear relaxation and 2 for the bulk relaxation.

Glass is a thermorheologically simple material. This means that the relaxation time at different temperatures can be calculated with a shift function ϕ. The relaxation time τ is temperature dependent and it can be presented with the Arrhenius equation, where *H* is the activation energy and *R* is the gas constant (Scherer 1986). In the equation of the shift function units of temperatures are [K].

$$\phi(t) = \frac{\tau_{ref}}{\tau} = \frac{\eta_{ref}}{\eta} = \exp\left[\frac{H}{R}\left(\frac{1}{T_{ref}} - \frac{1}{T}\right)\right] \tag{3.28}$$

The relaxation functions can be written in terms of the reduced time ξ which is obtained from equation (Scherer 1986)

$$\xi(t) = \int_0^t \phi\big(T(t')\big) dt' \tag{3.29}$$

and the constitutive equation (3.25) can be presented as

$$\sigma_{ij}(t) = \delta_{ij} \int_0^t K\big(\xi(t) - \xi(t')\big) \frac{\partial(\bar{\varepsilon} - 3\varepsilon^{th})}{\partial t'} dt' + 2 \int_0^t G\big(\xi(t) - \xi(t')\big) \frac{\partial e_{ij}}{\partial t'} dt' \tag{3.30}$$

3.2.3. Structural relaxation

At low temperatures, below the transition temperature, glass is in an unstabilized state. A glass is said to be stabilized when it has been held at a given temperature until the properties have stopped changing with the time (Scherer 1986). Structural relaxation refers to the arrangement of the microstructure of the material, which is changing over the time (Nielsen 2008). The changes in properties such as thermal expansion coefficient, specific heat and relaxation times are dependent on the fictive temperature T_f and those can be described with the response function

$$M_p(t) = \frac{p(t) - p_2(\infty)}{p_2(0) - p_2(\infty)} = \frac{T_f(t) - T_2}{T_1 - T_2} \tag{3.31}$$

In the response function M_p above p is a property and the subscript 1 is the state before the temperature change and 2 is the state after the temperature change. The fictive temperature can be calculated using Eq. (3.31). The whole time history has to be taken into account because the temperature change is time-dependent

$$T_f(t) = T(t) - \int_0^t M_p(t - t') \frac{\partial T}{\partial t'} dt' \tag{3.32}$$

Where $\partial T/\partial t' = q_{cr}$ is the heating or cooling rate.

The response function of the material property M_p can be expressed by analogy with the bulk or shear relaxation function

$$M_p(t) = \sum_{r=1}^{R} C_r \exp\left(-\frac{t}{\lambda_r}\right) \tag{3.33}$$

where λ_r is a relaxation time and C_r is a weight coefficient (Scherer 1986).

Due to the structural relaxation of the material, the shift function ϕ also changes. It is the combination of temperature and the fictive temperature

$$\phi(t) = \exp\left[\frac{H_g}{R}\left(\frac{1}{T_{ref}} - \frac{1}{T}\right) + \frac{H_s}{R}\left(\frac{1}{T_{ref}} - \frac{1}{T_f}\right)\right] = \exp\left[\frac{H}{R}\left(\frac{1}{T_{ref}} - \frac{x}{T} - \frac{1-x}{T_f}\right)\right] \tag{3.34}$$

In Eq. (3.34) the activation energy $H = H_g + H_s$ and $x = H_g/H$, where H_g is related to the temperature and H_s to the structure.

The thermal strain depends on the change in temperature and the fictive temperature as a function of time

$$\varepsilon^{th}(t) = \left(\alpha_l - \alpha_g\right)\left(T_f(t) - T_f(0)\right) + \alpha_g\left(T(t) - T(0)\right) \tag{3.35}$$

where α_l is the thermal expansion coefficient for the liquid state and α_g for the glassy state. In a liquid state the expansion coefficient is about three times the expansion coefficient in a glassy state for a soda-lime glass and it has a major influence on stress forming.

The property change is dependent on the speed of the temperature change. This can be seen in Fig 3.4. When cooling at a faster rate, the time for relaxation of a property shortens. Thus, the effect of structural change decreases at high temperature. The difference can be observed from the fictive temperature curves. The constant value of the fictive temperature after cooling shows the glass transition temperature. With a higher cooling rate q_{cr} the transition temperature T_g is higher. The change of transition temperature due to the cooling rate can also be seen in Eq. (3.36) (Scherer 1986)

$$\frac{d(1/T_g)}{d(\ln q_{cr})} = -\frac{R}{H} \tag{3.36}$$

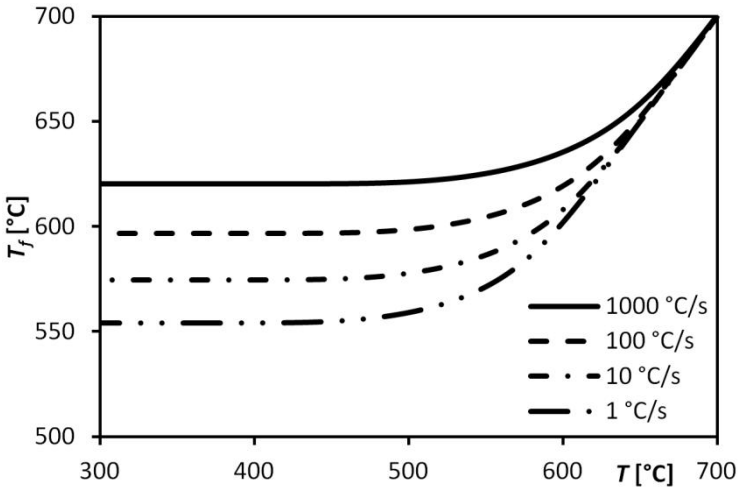

Figure 3.4. Effect of cooling rate on fictive temperature.

4. NUMERICAL MODELLING

4.1. Heat transfer

The modelling of a tempering process needs the temperature field as a basis in the stress analysis. In the simplest case a 1D treatment is adopted in which phenomena in the thickness direction only are examined. In this case the edge behaviour is ignored. The temperature field can be calculated using an implicit or explicit finite difference method. Glass is divided into layers where the nodes are in the centre of each control volume except at the surface. In the entire control volume the same thermal properties are assumed as in the node. The distance between nodes can vary through the thickness. In the explicit method the maximum size of the time step depends on the maximum distance between nodes. These types of restrictions are not encountered if use is made of an implicit method. The implicit method was thus chosen. With the shorter distance between nodes on the surface, the accuracy of heat transfer calculation with strong convection can be increased. Figure 4.1 shows the computational grid.

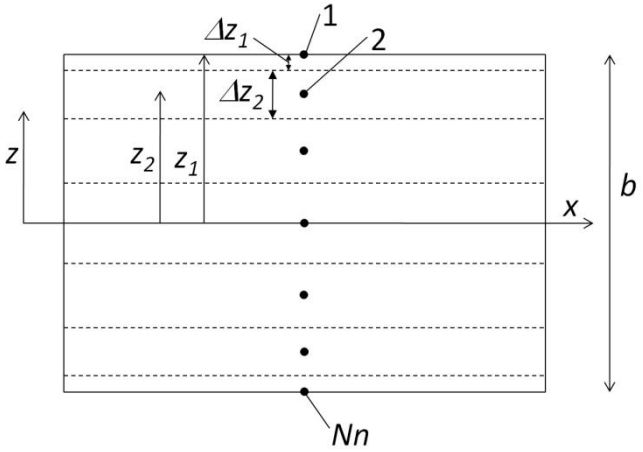

Figure 4.1. Nodes and control volumes in 1D calculation.

4.2. Viscoelasticity

When the temperature field is known from Eq. (3.1), the stress field can be calculated. In the calculation of stress field, the same computational grid and assumptions for material properties in the whole control volume can be used. The calculation of stresses is quasi-static. The temperature and material properties are known at a given time. Eq. (3.30) has been used for the calculation of stresses. Because the relaxation is described with exponential functions, the hereditary integral can be evaluated incrementally and the stress history can be updated recursively (Chambers 1992)

$$\sigma_{ij}(t_n) = \delta_{ij}\frac{1}{3}\bar{\sigma}(t_n) + s_{ij}(t_n) \tag{4.1}$$

$$\bar{\sigma}(t_n) = \sum_{p=1}^{P} \bar{\sigma}^p(t_n) + 3K_\infty[\bar{\varepsilon}(t_n) - 3\varepsilon^{th}(t_n)] \tag{4.2}$$

$$s_{ij}(t_n) = \sum_{q=1}^{Q} s_{ij}^q(t_n) \tag{4.3}$$

$$\bar{\sigma}^p(t_n) = exp\left\{-\frac{[\xi(t_n) - \xi(t_{n-1})]}{\tau_{2p}}\right\}\bar{\sigma}^p(t_{n-1}) + (3K_0 - 3K_\infty)w_{2p}k_p(\Delta t_n)\{[\bar{\varepsilon}(t_n) - \bar{\varepsilon}(t_{n-1})] - [3\varepsilon^{th}(t_n) - 3\varepsilon^{th}(t_{n-1})]\} \tag{4.4}$$

$$s_{ij}^q(t_n) = exp\left\{-\frac{[\xi(t_n) - \xi(t_{n-1})]}{\tau_{1q}}\right\}s_{ij}^q(t_{n-1}) + 2G_0 w_{1q} g_q(\Delta t_n)\left\{[\varepsilon_{ij}(t_n) - \varepsilon_{ij}(t_{n-1})] - \frac{\delta_{ij}}{3}[\bar{\varepsilon}(t_n) - \bar{\varepsilon}(t_{n-1})]\right\} \tag{4.5}$$

$$k_p(\Delta t_n) = \frac{1}{\Delta t_n}\int_{t_{n-1}}^{t_n} \exp\left\{-\frac{[\xi(t_n) - \xi(t')]}{\tau_{2p}}\right\}dt' \tag{4.6}$$

$$g_q(\Delta t_n) = \frac{1}{\Delta t_n}\int_{t_{n-1}}^{t_n} \exp\left\{-\frac{[\xi(t_n) - \xi(t')]}{\tau_{1q}}\right\}dt' \tag{4.7}$$

If the reduced time $\xi(t)$ is assumed to vary linearly over the time step Δt_n the integral expressions in Eqs. (4.6) and (4.7) can then be approximated as

$$k_p(\Delta t_n) = \frac{\tau_{2p}}{\Delta\xi_n}\left\{1 - \exp\frac{-\Delta\xi_n}{\tau_{2p}}\right\} \tag{4.8}$$

$$g_q(\Delta t_n) = \frac{\tau_{1q}}{\Delta\xi_n}\left\{1 - \exp\frac{-\Delta\xi_n}{\tau_{1q}}\right\} \tag{4.9}$$

where $\Delta\xi_n$ is the difference of reduced time over time step Δt_n.

$$\Delta\xi_n = \xi(t_n) - \xi(t_{n-1}) \tag{4.10}$$

The equilibrium equations (3.16) and (3.17) can be integrated by using the sum equation or the trapezoidal rule if the distance between nodes is uniform

$$\int_{-b/2}^{b/2} \sigma_{xx}\,dz = \sum_{i=1}^{Nn} \sigma_{xx}^i \Delta z_i \tag{4.11}$$

$$\int_{-b/2}^{b/2} \sigma_{xx} z dz = \sum_{i=1}^{Nn} \sigma_{xx}^{i} z_i \, \Delta z_i \tag{4.12}$$

In these equilibrium equations σ_{xx}^{i} is the stress on node *i*, Δz_i is the thickness of control volume *i* and z_i is the z coordinate of node i.

By substituting Eqs. (4.2) – (4.7) in Eq. (4.1) and Eq. (4.1) in Eqs. (4.11) and (4.12), then the mid-plane strain ε_{xx}^{0} and the curvature κ_x in x and y directions are the only unknowns. The mid-plane strain ε_{xx}^{0} can be solved with the equilibrium equation (4.11) and the curvature $\kappa_x$with Eq. (4.12).

4.3. Structural relaxation

The fictive temperature (Eq. (3.32)) and the shift function (Eq. (3.34)) can be calculated by using the explicit algorithm of Markovsky & Soules (1984)

$$T_{f_r}(t) = \frac{\lambda_r T_{f_r}(t - \Delta t) + \Delta t T(t) \phi(t)}{\lambda_r + \Delta t \phi(t)} \tag{4.13}$$

$$T_f(t) = \sum_{r=1}^{n} C_r T_{f_r}(t) \tag{4.14}$$

$$\phi(t) = \exp\left[\frac{H}{R}\left(\frac{1}{T_{ref}} - \frac{x}{T} - \frac{1-x}{T_f(t-\Delta t)}\right)\right] \tag{4.15}$$

The initial value for the fictive temperature has to be fixed. If the initial temperature is higher than the glass transition temperature, then $T_f(0)=T(0)$. Otherwise the initial fictive temperature is the glass transition temperature of an annealed glass. In this study equal to 550 °C.

Because the fictive temperature has an effect on the specific heat, shown in Eq. (3.7), the fictive temperature and the shift function have to be calculated during the temperature field calculation.

The increment of reduced time can be calculated using the trapezoidal integration rule

$$\Delta\xi = \int_{t}^{t+\Delta t} \phi(t') dt' = \frac{\Delta t}{2}[\phi(t + \Delta t) - \phi(t)] \tag{4.16}$$

4.4. Treatment of stresses and boundary conditions

The boundary conditions for mechanical behaviour should be known. In the case of a large glass plate the plane stress assumption in the z direction is an appropriate choice.

There can also be other approaches such as a plane strain assumption, or it may be assumed that the thickness change depends only on the thermal strain. In Fig. 4.2 the results of the surface and mid-plane transient stresses with different boundary conditions in z direction are shown. The results are calculated by using the equations above. In the plane stress $\sigma_{zz} = 0$, in the plane strain $\varepsilon_{zz} = 0$ for a plate. In the third case the thickness of an element is dependent only on the thermal strain $\varepsilon_{zz} = \varepsilon^{th}$ for a plate.

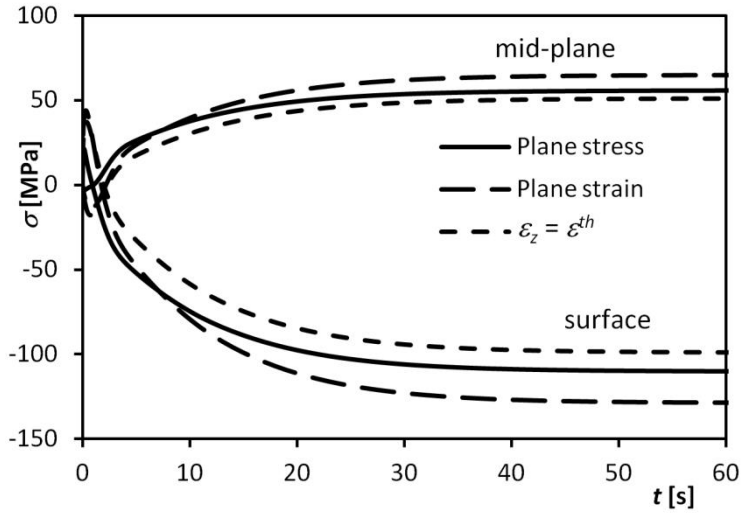

a)

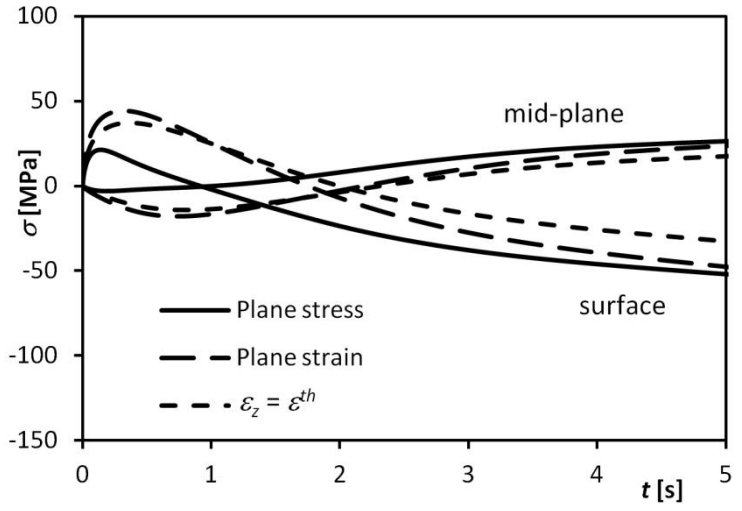

b)

Figure 4.2. Transient stress history distribution with different boundary conditions in z direction. b = 3 mm, T_0 = 650 °C and h = 600 W/m^{2}K. (a) whole transient stress history and (b) beginning of cooling (5 s).

In the x and y directions behaviour is different from that in the z direction. The most functional boundary equations for those directions are the normal force and moment equations

$$\int_{-b/2}^{b/2} \sigma_{xx} dz = N_x \tag{4.17}$$

$$\int_{-b/2}^{b/2} \sigma_{xx} z dz = M_x \tag{4.18}$$

For a free plate the normal force N_x and moment M_x are both zero. In the supported case the moment and the normal force can depend on the support and on the plate weight.

4.5. Displacements

When strain and curvature equations are solved, they are used to solve the displacements *u*, *v* and *w* which are in x, y and z directions, as follows

$$u(x,y,z,t) = \int_0^x (\varepsilon_{xx}^0(x,y,t) + \kappa_x(x,y,t)z) dx \tag{4.19}$$

$$v(x,y,z,t) = \int_0^y \left(\varepsilon_{yy}^0(x,y,t) + \kappa_y(x,y,t)z\right) dy \tag{4.20}$$

$$w(x,y,z,t) = \int_0^x \int_0^x \kappa_x(x,y,t) dx\, dx + \int_0^y \int_0^y \kappa_y(x,y,t) dy\, dy + \int_0^z \varepsilon_{zz}(x,y,z,t) dz \tag{4.21}$$

These equations are valid for the case shown in Fig. 3.2, if the plate is fully supported and rotation is restricted to point (0,0,0).

5. TRANSIENT AND RESIDUAL STRESSES

The one-dimensional program has been developed during this work for the simulation of the residual stress profile. With one-dimensional calculations it is easy to study the effect of the main parameters and material properties on glass behaviour. In addition, if the loading of a glass plate is known, the effect of temperature, material properties and loading on deformations can be studied. This chapter presents the transient and residual stresses calculated with the one-dimensional program for a free plate. The effect of support on deformations is discussed in Chapter 6.

5.1. Comparison of stress calculations

The mid-plane residual stresses measured by Gardon and the simulation results of this study with the one-dimensional code are shown in Fig. 5.1. Physical properties used are given in the Appendix A. In this case the glass thickness is 6.1 mm and the initial temperatures and heat transfer coefficients vary. Radiation is also included inside the glass. The shapes of curves with a small heat transfer coefficient are similar, but with high heat transfer coefficients the simulated stress state is about 10 % lower. In Fig. 5.2 the stress ratio between the surface compression and mid-plane tension is shown for the same cases as in Fig. 5.1. The results agree quite well with each other.

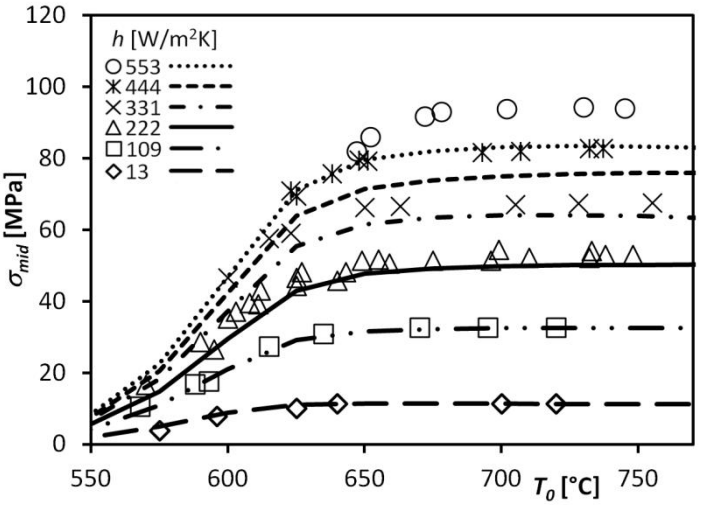

Figure 5.1. Comparison of experimental (points (Gardon 1965)) and calculated (lines) results for mid-plane residual stresses with different initial temperatures and heat transfer coefficients. Glass thickness is 6.1 mm.

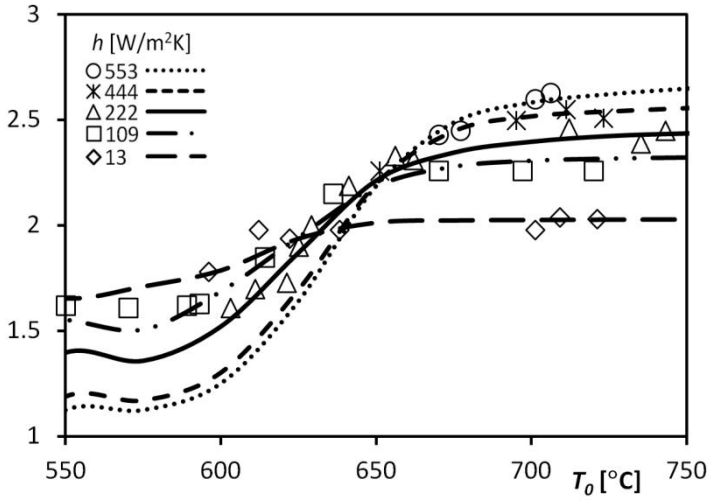

Figure 5.2. Comparison of experimental (points (Gardon 1980)) and calculated (lines) results for ratio of surface residual stress and mid-plane residual stress with different initial temperature and heat transfer coefficients. Glass thickness is 6.1 mm.

The reason for the difference between the experimental results by Gardon and the simulated results could be caused by different values for the material properties. The results in Fig. 5.1 are very sensitive to the values of the material properties (Nielsen 2010b, Aronen & Karvinen 2011). The effect of variations in material properties is discussed in Chapter 5.4. Another reason may also be the inaccuracy of heat transfer coefficient and stress measurements.

5.2. Effect of temperature and heat transfer coefficient

With the 1D program the influence of tempering parameters, i.e. the initial temperature before cooling and the heat transfer coefficient during cooling, on the transient and residual stresses can be investigated. In this case all the external forces are ignored, glass is freely supported, and the plate is assumed to be large so that stresses in the x and y directions are the same.

During cooling, the temperature difference between the surface and mid-plane must be over 130 °C in order to create the required stress (more than 80-100 MPa compression on the surface). The behaviour of the tempering process depends on the glass thickness. The required convective heat transfer coefficient depends on the glass thickness. Moreover, the value of the convective heat transfer coefficient affects the cooling rate and structural relaxation.

The effect of tempering parameters is studied with three different thicknesses equal to 2 mm, 4 mm and 10 mm. The temperature range in simulations was from 550 °C to 750 °C or more. In Figs. 5.3 – 5.5 the effect of temperature and heat transfer coefficients on

surface residual stress is shown. The surface residual stress is the most important factor in terms of tempering quality.

The values of temperatures and heat transfer coefficients are presented in non-dimensional form. The reference value of temperature T_r is obtained from Eq. (3.32) using cooling rate 100 °C/s. Then the glass transition temperature T_g and the reference temperature T_r is about 600 °C. In Figs 5.3-5.11 temperatures are in [°C]. The reference value of heat transfer coefficient h_r is the heat transfer coefficient needed to reach 120 MPa surface compressive residual stress at temperatures above the plateau-level for 3 mm glass. This is discussed in detail below.

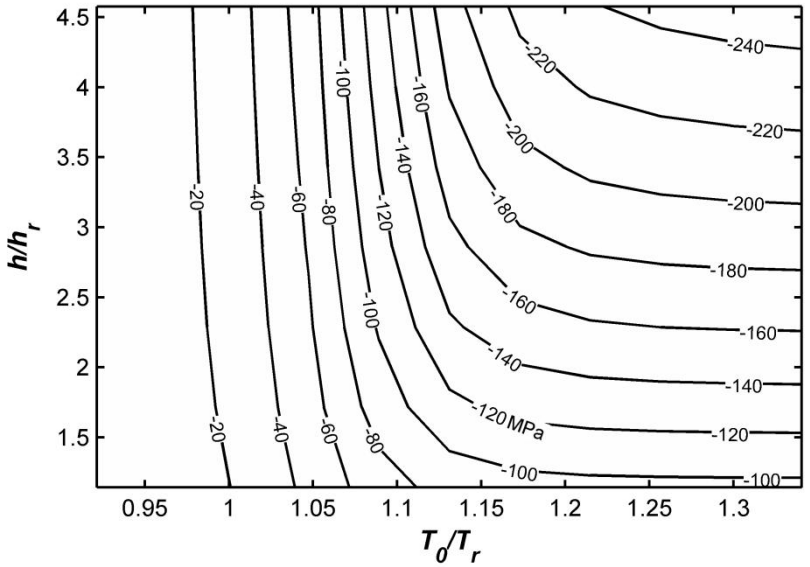

Figure 5.3. Effects of temperature and heat transfer coefficient on surface residual stress. Glass thickness is 2 mm.

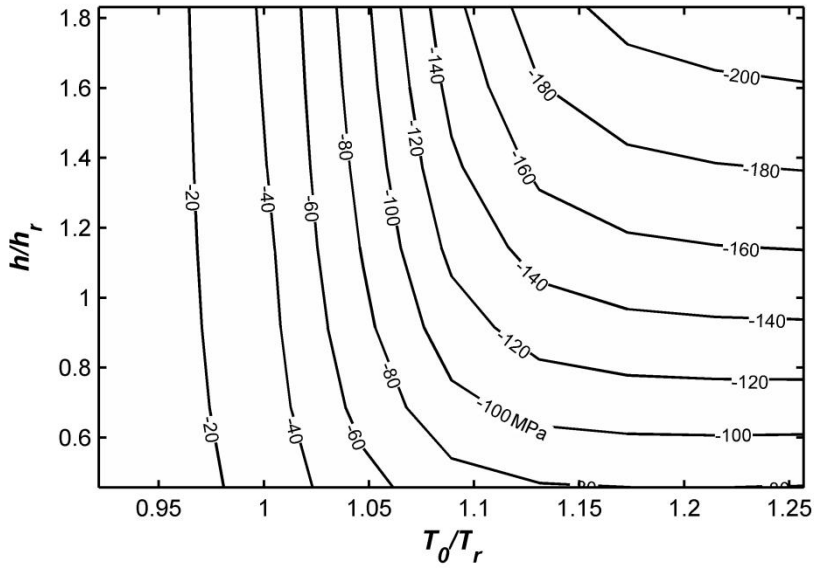

Figure 5.4. Effects of temperature and heat transfer coefficient on surface residual stress. Glass thickness is 4 mm.

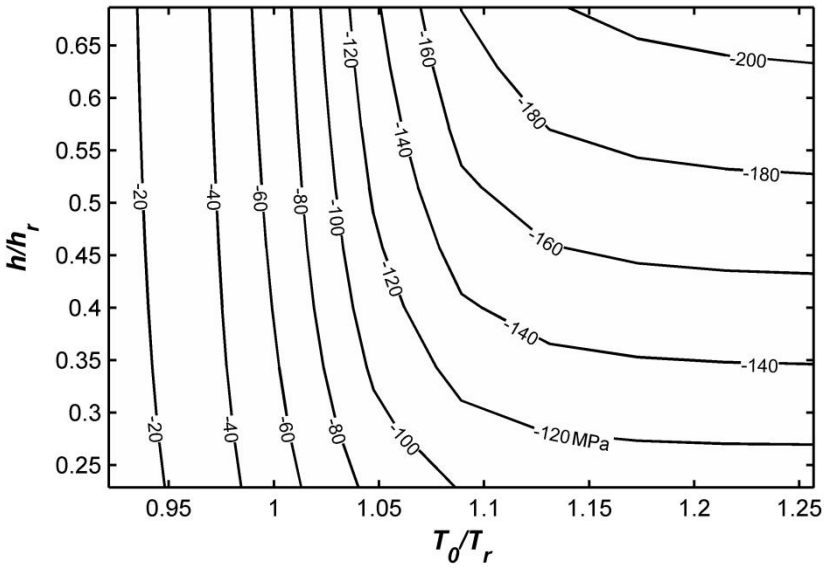

Figure 5.5. Effects of temperature and heat transfer coefficient on surface residual stress. Glass thickness is 10 mm.

High values of temperature and heat transfer coefficients make the tempering easier. When the temperature is high, the relaxation speed increases and more viscous strain is generated. When the temperature differences disappear, residual stresses are created due to the viscous strains. With a low temperature, the relaxation can be too slow and only elastic strains occur.

With higher heat transfer coefficients, the temperature difference between the surface and the mid-plane is increased. At temperatures below 600 °C the viscosity is too high to create the necessary viscous strains and the increase of the heat transfer coefficient does not affect residual stresses. On the other hand, at temperatures above 650 - 700 °C the relaxation is fast enough to create viscous strains and the plateau-level is reached. Thus, the level of residual stress depends on the temperature differences during the cooling. The plateau-level is reached when the temperature increase does not change the residual stress.

The effect of tempering parameters on the mid-plane residual stresses is quite similar to the surface residual stresses. The results are shown in Figs. 5.6 - 5.8. The only difference between surface and mid-plane stresses is that the plateau level is reached at a temperature level about 50 °C lower.

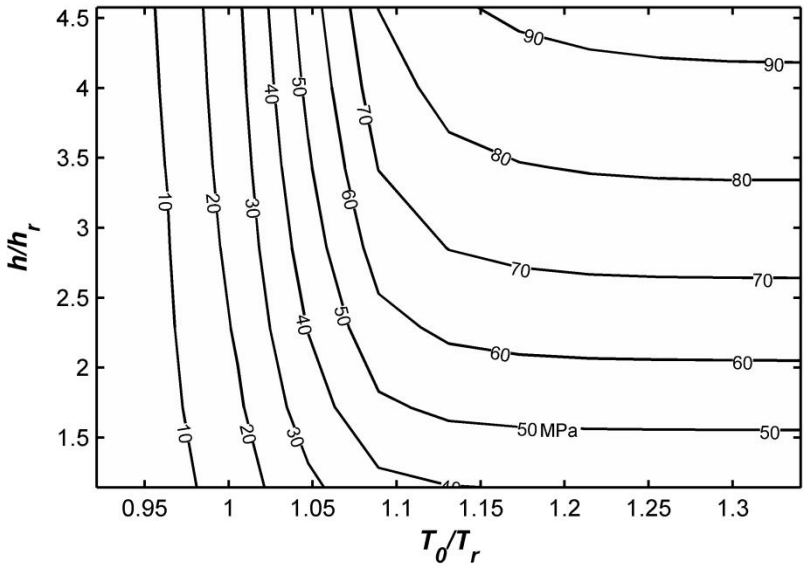

Figure 5.6. Effects of temperature and heat transfer coefficient on mid-plane residual stress. Glass thickness is 2 mm.

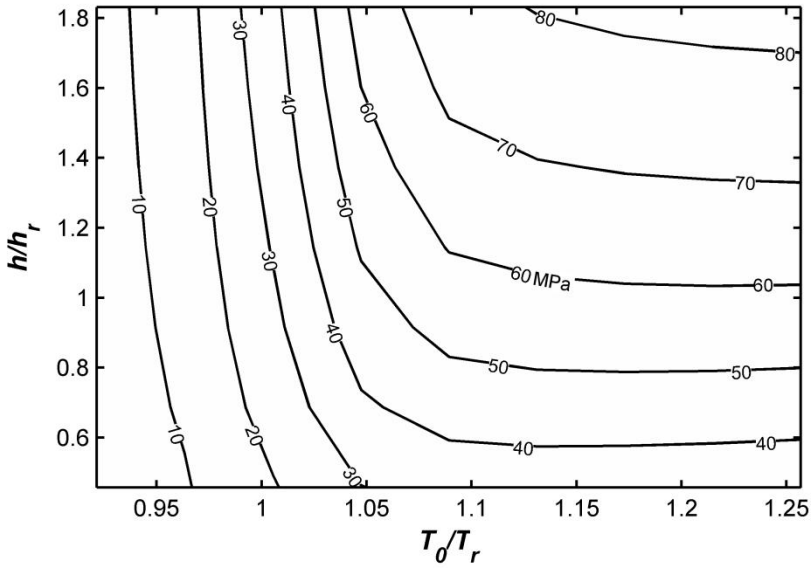

Figure 5.7. Effects of temperature and heat transfer coefficient on mid-plane residual stress. Glass thickness is 4 mm.

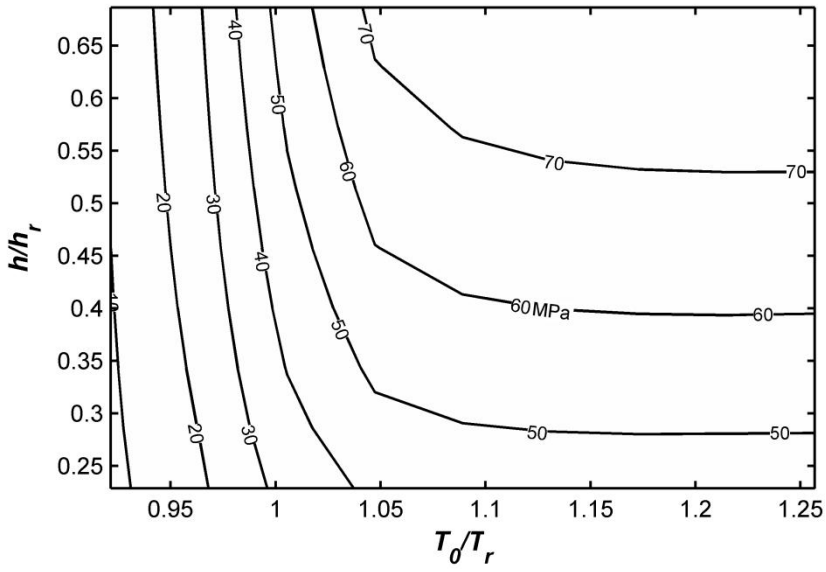

Figure 5.8. Effects of temperature and heat transfer coefficient on mid-plane residual stress. Glass thickness is 10 mm.

In an elastic case, the cooling of the surface creates the tensile stress in the surface at the onset of cooling. Due to the viscoelasticity, the tensile stress is created, but it is reduced by the relaxation of stresses at the high temperature. It is important to keep tensile stress as low as possible to prevent the fragmentation of glass due to the tensile stress during cooling. Figures 5.9 – 5.11 show the effect of tempering parameters on maximum tensile stress in the surface during cooling. The maximum allowable tensile stress of material depends on the surface quality and is approximately between 30 and 50 MPa at the edges.

Temperature is the most important parameter affecting the tensile stress during cooling. With lower temperatures, the tension forms in the surface at the onset of cooling. The temperature level affects the viscosity and with high viscosity the stresses do not relax. With a higher initial temperature the high tension in the surface at the beginning of cooling can be prevented. The most important temperature range is from 600 °C to 650 °C. The heat transfer coefficient has only a minor influence on the tensile stress created during cooling, as can be seen in Figs. 5.9 – 5.11.

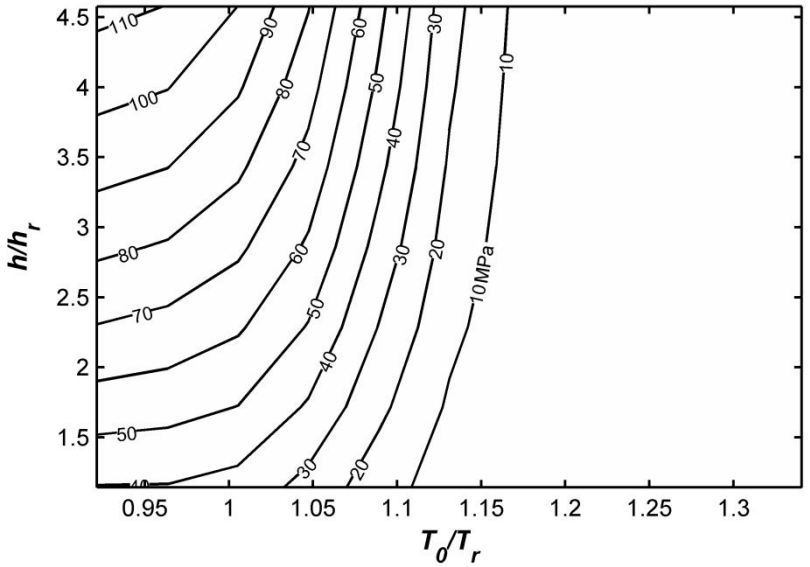

Figure 5.9. Effects of temperature and heat transfer coefficient on surface maximum tensile stress. Glass thickness is 2 mm.

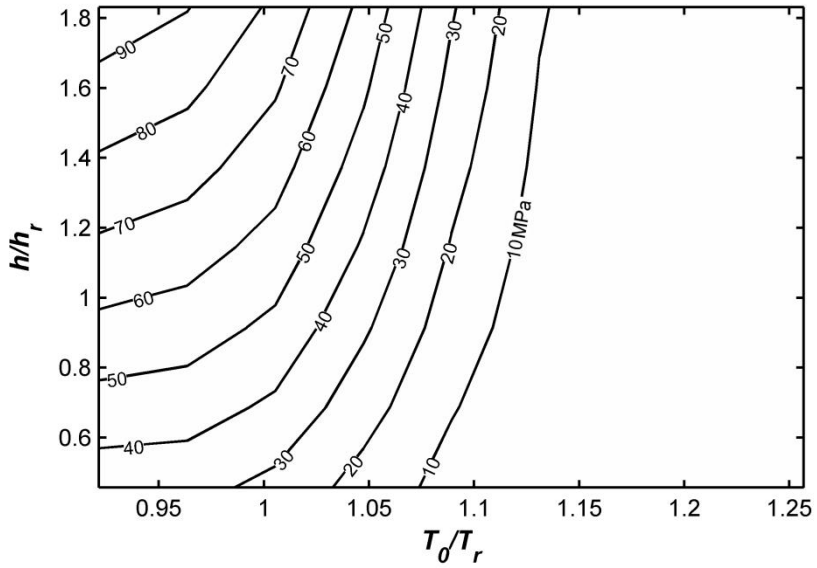

Figure 5.10. Effects of temperature and heat transfer coefficient on surface maximum tensile stress. Glass thickness is 4 mm.

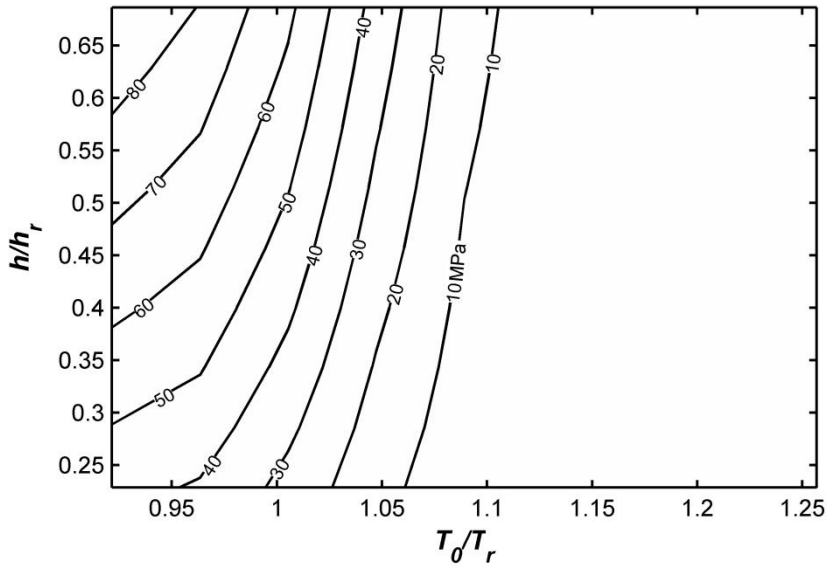

Figure 5.11. Effects of temperature and heat transfer coefficient on surface maximum tensile stress. Glass thickness is 10 mm.

5.3. Effect of modified cooling

During the quenching of glass the beginning of cooling is the most important factor related to residual stresses. When the glass temperature is dropped below the transition temperature, the convective heat transfer coefficient can be changed without significant changes in residual stresses. The benefit of increasing or decreasing the heat transfer coefficient is that the power of the blowers can be reduced or the cooling time can be shortened. The upper limit for the heat transfer coefficient is set by the surface tension and the lower one by residual stresses.

In tempering of thin glass, heat transfer necessitates high energy consumption by blowers. The time required for the heat transfer coefficient to remain high is short and after quenching, the heat transfer rate is usually reduced for cooling. The effect of the switch time of heat transfer coefficient on transient and residual stresses was studied by using a one-dimensional program. Figure 5.12 presents the residual stresses when the rate of heat transfer was changed at different times. The heat transfer coefficient at the beginning h_1 is 900 W/m^{2}K and after a time t_1 it was switched to h_2. Figure 5.13 shows the effect of the switch time, $t_{1,}$ on the maximum tensile stress at the surface. In the simulations, the initial temperature is 660 °C for 2 mm thick glass.

From the results in Fig. 5.12 it can be seen that after two seconds, heat transfer has no effect on residual stresses with the heat transfer coefficients tested. To change the maximum tensile stress at the surface the switch time should be less than 0.2 s with the heat transfer coefficients tested, as shown in Fig. 5.13.

In the tempering of thick glass, the heat transfer coefficient is required to increase in order to reduce the cooling time. Figure 5.14 shows that the heat transfer coefficient should remain constant for over 20 seconds to avoid changes in the residual stresses. The effect of switch time t_1 on surface maximum tensile stress is shown in Fig. 5.15. With 10 mm thick glass the initial temperature is 630 °C and the heat transfer coefficient at the beginning h_1 is 200 W/m^{2}K.

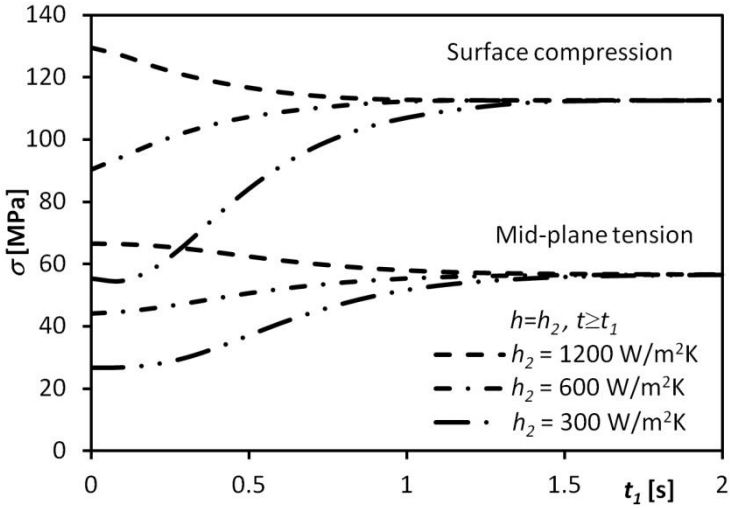

Figure 5.12. Effect of switch time of heat transfer coefficient t_1 on residual stresses. Glass thickness is 2 mm, h_1 = 900 W/m^{2}K and T_0 = 660 °C.

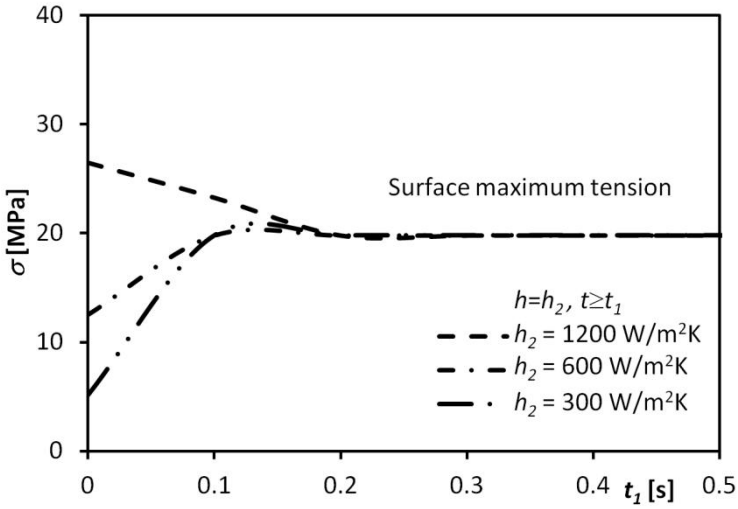

Figure 5.13. Effect of switch time of heat transfer coefficient t_1 on surface maximum tensile stress. Glass thickness is 2 mm, h_1 = 900 W/m^{2}K and T_0 = 660 °C.

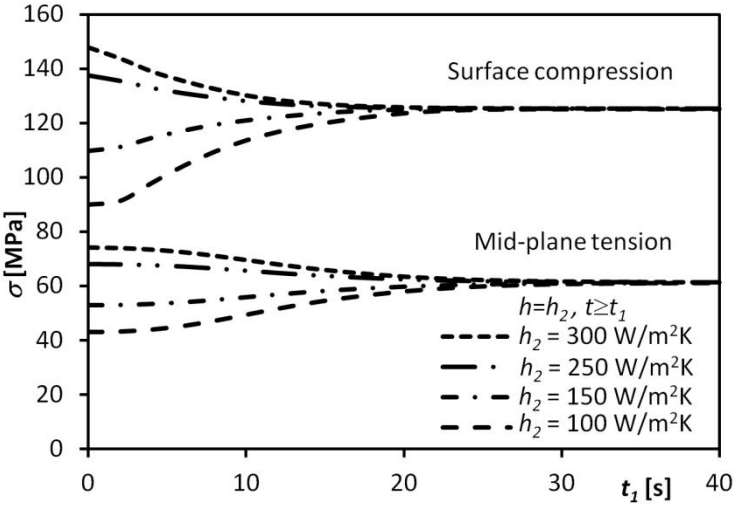

Figure 5.14. Effect of switch time of heat transfer coefficient t_1 on residual stresses. Glass thickness is 10 mm, h_1 = 200 W/m^{2}K and T_0 = 630 °C.

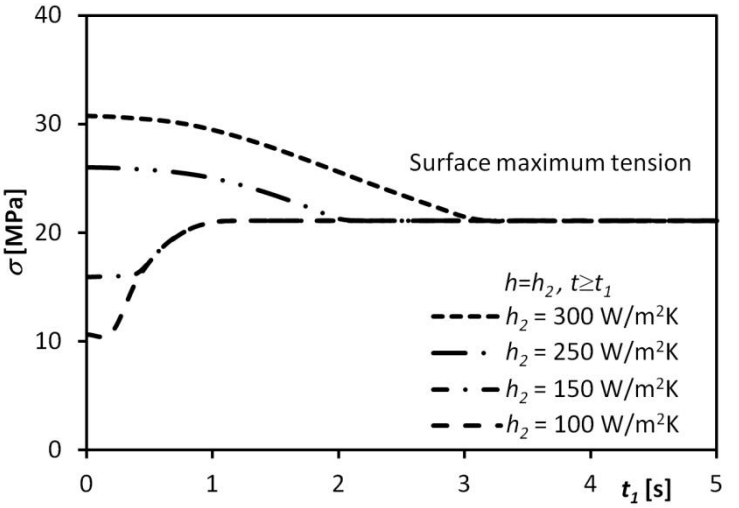

Figure 5.15. Effect of switch time of heat transfer coefficient t_1 on surface maximum tensile stress. Glass thickness is 10 mm, h_1 = 200 W/m^{2}K and T_0 = 630 °C.

5.4. Effect of material properties on residual stresses

In simulations the values of material properties are important. However, at high temperatures the measuring of material properties is difficult and they vary from reference to reference. Glass has many temperature dependent material properties which have different effects on the simulation results for the tempering process. With the sensitivity analysis, the effect of material properties on stresses can be studied.

Values of three material properties are needed in heat transfer calculations, namely, specific heat, thermal conductivity and density. Four are needed in the modelling of mechanical behaviour: Young's modulus, Poisson's ratio, thermal expansion coefficient and viscosity. The reported property values found in the literature and used in simulations varied by as much as 20 %, depending on the property concerned. Simulations were undertaken for the 4 mm thick glass. The reference values are shown in Appendix A.

When considering the material property values in the literature and the results below, it can be seen that the change in measured values of material properties can vary by over 20 % between different references. When looking for the most sensitive material properties such as thermal conductivity and thermal expansion coefficients, the literature values vary markedly, perhaps due to the fact that they are difficult to measure at high temperatures.

5.4.1. Thermal properties

Heat transfer and the temperature field control the tempering process and they also have a major influence on the stress field. Three material properties govern the forming of the temperature field.

Figure 5.16 shows the influence of thermal material properties on the surface residual stresses. In simulations the initial temperature was 650 °C and the heat transfer coefficient equal to 500 W/m^{2}K. With the reference material properties shown in Appendix A, the surface residual stress is 124.9 MPa. In the results, the abscissa shows the ratio of modified material property value p and the reference value p_A shown in the Appendix A (p/p_A) and the ordinate shows the change of residual stress $(\sigma - \sigma_A)/\sigma_A$.The reference residual stress σ_A is calculated using the material values shown in the Appendix A.

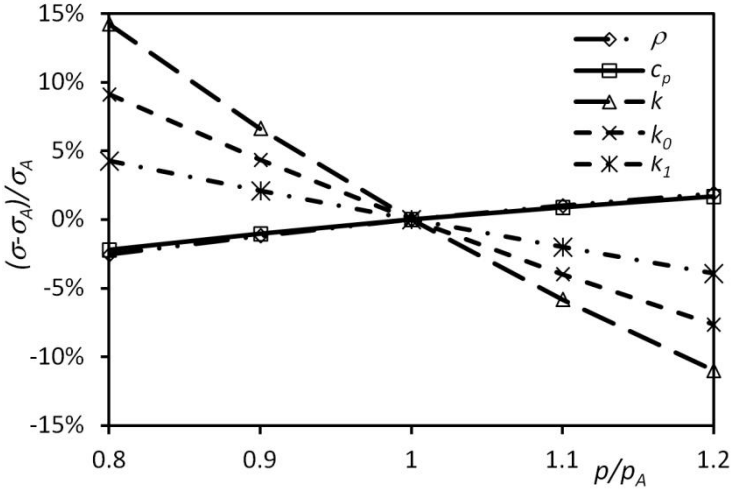

Figure 5.16. Surface residual stress changes at 650 °C and h = 500 W/m^{2}K with different thermal properties. On abscissa p represents property value. Glass thickness is 4 mm.

The density changes only slightly during the process and it can be assumed to be constant. It does not have a significant influence on the residual stresses. With lower density glass, temperature drops faster and the glass has less time for stress relaxation, resulting in a decrease in residual stresses.

The specific heat is nonlinearly temperature dependent and depends on the phase change over the transition range. The calculation of specific heat can be divided into two parameters: specific heat in the glassy state and in the liquid state. In the glassy state specific heat is temperature dependent but in the liquid state it is almost constant. The calculated results are almost the same when density or specific heat are changed from the reference values shown in Appendix A (dots ◇ and □ in Fig 5.16).

The thermal conductivity is linearly dependent on temperature.

$$k(T) = k_0 + k_1 T \tag{5.1}$$

It has a major influence on the residual stresses. Figure 5.16 shows that a 10 % increase in thermal conductivity k can decrease residual stresses by over 5 %. The thermal conductivity has a big influence on residual stresses, because it affects the temperature difference between the surface and the mid-plane. With higher thermal conductivity the temperature field is more even. The effect of the change of thermal conductivity on residual stresses depends on the initial temperature and the heat transfer coefficient. Figure 5.17 shows the effect of a 10 % increase in thermal conductivity on the surface residual stress as a function of the initial temperature and the heat transfer coefficient.

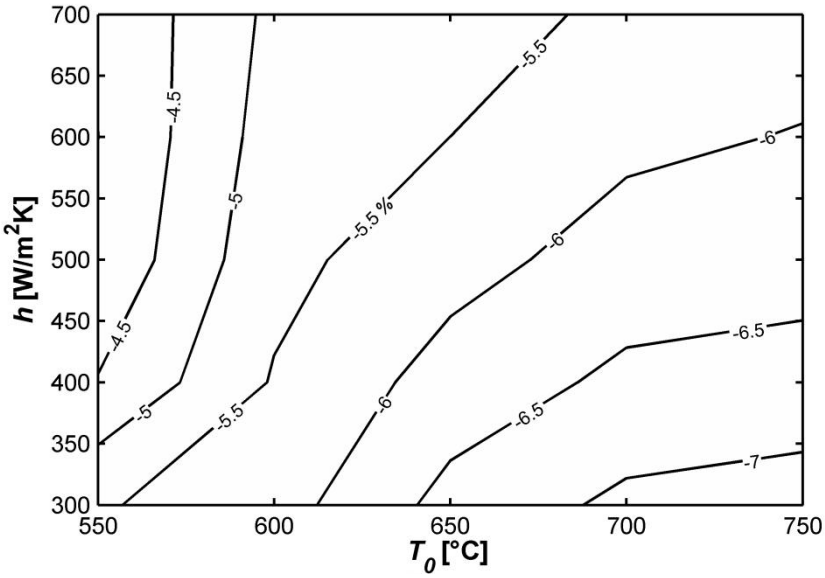

Figure 5.17. Effect of 10 % increase of thermal conductivity on surface residual stress as a function of the temperature and the heat transfer coefficient. Glass thickness is 4 mm.

In simulations the effect of total thermal conductivity k, constant part k_0 and temperature dependent part k_1 are studied separately. The results are shown in Fig. 5.16. The influence of the constant part is greater than the temperature dependent part.

5.4.2. Mechanical properties

Material properties that affect mechanical behaviour also have an influence on the creation of stress. There are four such properties: Young's modulus, Poisson's ratio, thermal expansion coefficient and viscosity. The effect of temperature on viscosity is presented with the help of Eq. (3.34) and the effect of viscosity on residual stresses is studied with the activation energy H/R, the ratio of structural and glassy activation energy x and the reference temperature T_{ref}.

In Fig. 5.18 the influence of mechanical material properties on surface residual stresses is shown. In simulations the property values presented in Appendix A were used as references.

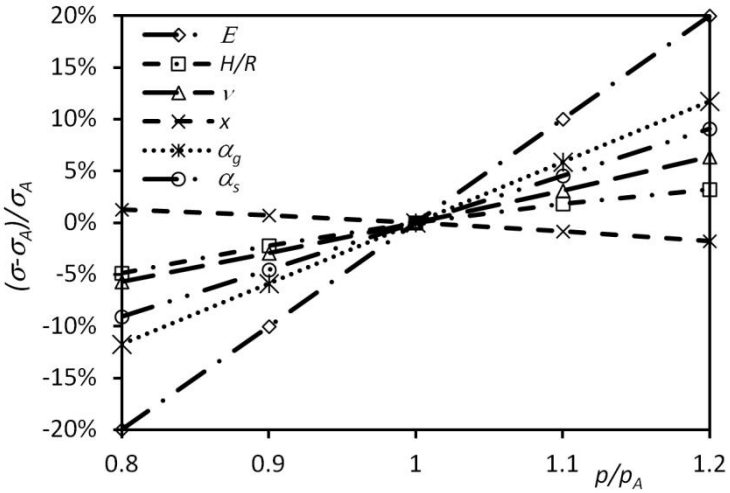

Figure 5.18. Surface residual stress changes at 650 °C and h = 500 W/m^{2}K with different mechanical properties. On abscissa p represents property value. Glass thickness is 4 mm.

The influence of Young's modulus is the easiest to see. The Young's modulus has an influence on the bulk and shear moduli. The change in the stress value is directly proportional to the Young's modulus.

The influence of Poisson ratio is more complicated. It affects both the bulk and shear moduli, but the coefficients are different for each modulus. The influence of the Poisson ratio is smaller than Young's modulus and a 10 % change in the Poisson ratio leads to changes of about 3 % in stresses.

The thermal expansion coefficient depends on temperature and phase change such as the specific heat. The thermal expansion can be divided into two parts: the values in the glassy state and in the liquid state. The thermal expansion in the liquid state is about three times the expansion in the glassy state. The effect of thermal expansion in the glassy state and the structural influence on thermal expansion α_s was studied. The structural influence on thermal expansion α_s is the difference between the thermal expansion in the liquid state and in the glassy state ($\alpha_s=\alpha_l-\alpha_g$). The change in the thermal expansion in the glassy state has more impact on stresses than the structural change. Figure 5.18 shows that a 10 % change in the thermal expansion coefficient in the glassy state changes residual surface stress by about 6 % while a 10 % change in the structural thermal expansion coefficient changes it by about 4 %.

Many parameters affect the viscosity: the activation energy H/R, the ratio of structural and glassy activation energy x and the reference temperature T_{ref}. The most important parameter is the reference temperature. The reference temperature for viscosity or relaxation depends on which temperature the reference viscosity or relaxation times are presented and this varies in the literature. Figure 5.19 shows that in the transition range (550 °C – 600 °C) the effect can be a more than 20 % decrease in the residual stress for a

1 % increase in the reference temperature (from 869 K to 877.7 K). At temperatures above the transition temperature, the change is much smaller. Figure 5.20 shows the effect of the reference temperature on surface residual stresses. The influence of the reference temperature is nonlinear.

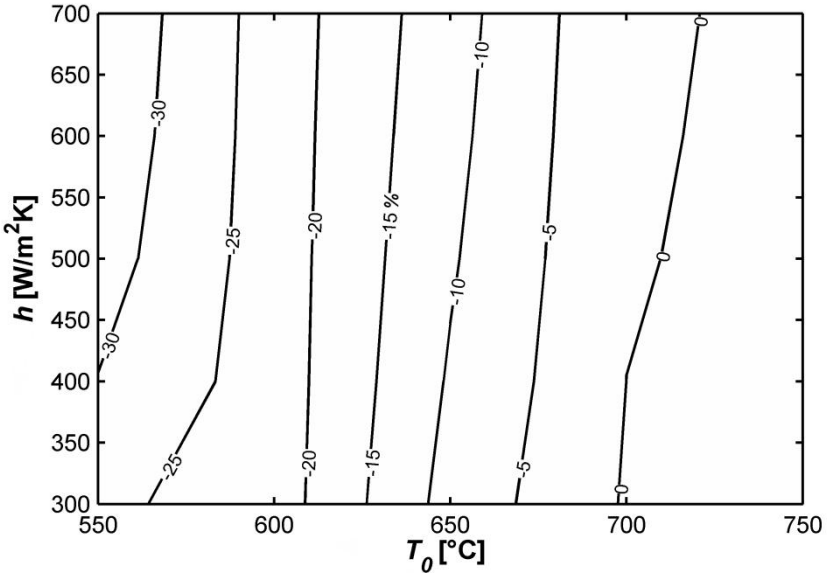

Figure 5.19. Effect of a 1 % increase in reference temperature on surface residual stress as a function of the temperature and the heat transfer coefficient. Glass thickness is 4 mm.

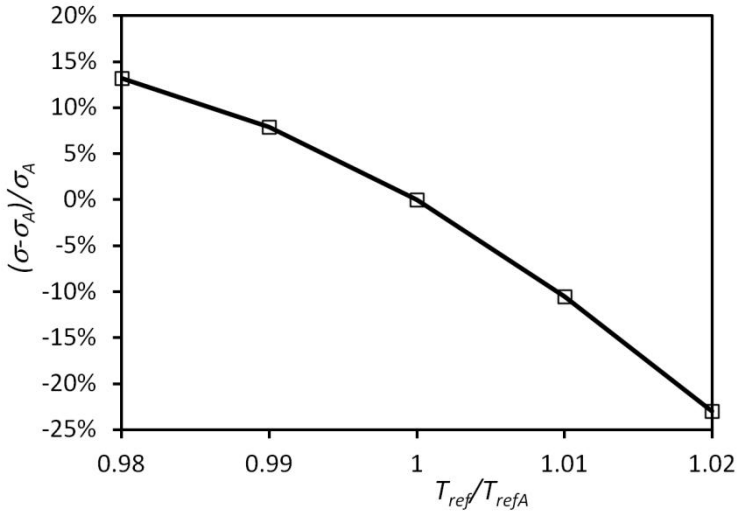

Figure 5.20. Surface residual stress changes at 650 °C and h = 500 W/m^{2}K with different T_{ref} values. Glass thickness is 4 mm.

Another important parameter in the case of relaxation is the activation energy. At the initial cooling temperatures near the transition range, the effect of the activation energy H/R and the ratio of structural and glassy activation energy x have an influence, but at the higher temperatures the effect can be neglected. The activation energy has more influence in the case of creeping at constant temperature, as shown in Chapter 6.

Other modifications tested, such as the infinite bulk modulus K_∞ and the ratio between the structural relaxation and shear relaxation λ_i/τ_{1i} have a very minor effect even with a ± 20 % change in the property.

5.5. Convergence of simulation

The convergence of residual stress simulations were tested for a glass with a thickness of 3 mm and an initial temperature of 650 °C and with the heat transfer coefficient equal to 600 W/m^{2}K.

5.5.1. Effect of node distance

The number of nodes and the distance between them have an effect on the accuracy of the temperature and stress results as well as on the calculation time. The number of nodes can be fairly small due to the thinness of glass plate. In Fig. 5.21 the effect of the number of nodes on different stress results is shown. The effect is studied for residual stresses on the surface and in the mid-plane as well as for the maximum transient stress on the surface and minimum transient stress in the mid-plane. The error in the residual stresses with only 21 nodes is small compared to calculations with a larger number of nodes. However, the calculation of maximum transient stresses on the surface needs more nodes.

In Fig. 5.22 the effect of ratio of the node distance between centre and surface is shown. It does not have a major effect on residual stresses although it does affect the temperature field at the beginning of cooling and then on the maximum surface tensile stress.

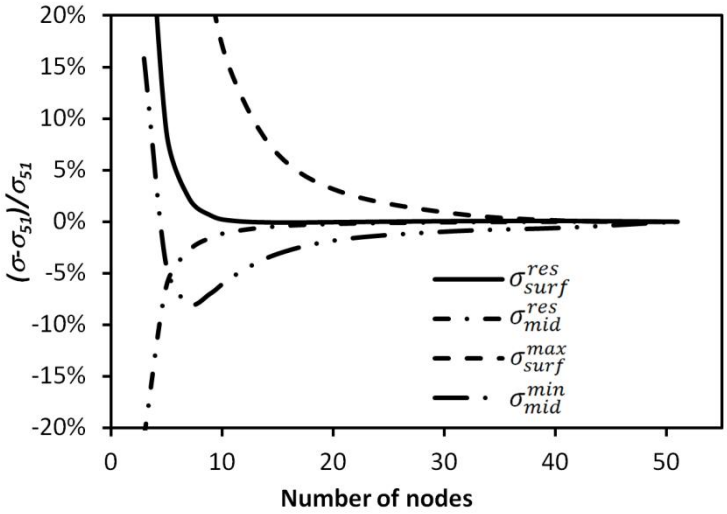

Figure 5.21. Effect of number of nodes on stresses. Reference σ_{51} with 51 nodes.

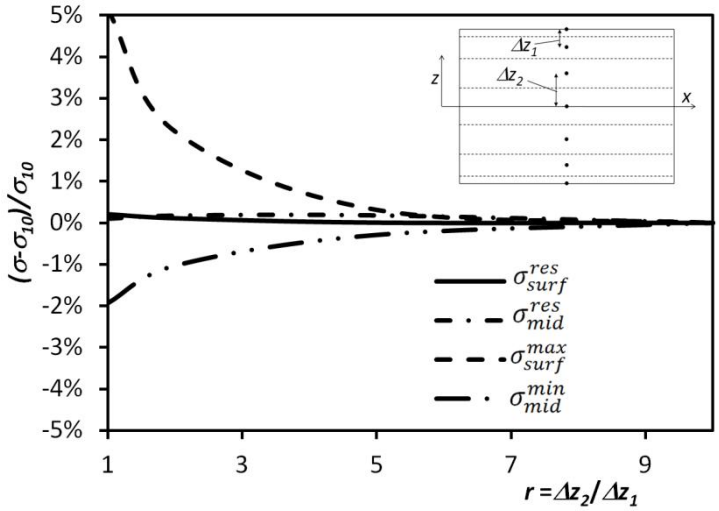

Figure 5.22. Effect of ratio $r = \Delta z_2/\Delta z_1$ on stress. Reference σ_{10}: number of nodes is 21 and r = 10.

5.5.2. Effect of time step

The time step also has an influence on the residual stresses. The effect of time step on the calculated results is hard to study because the initial temperature changes the results. By comparing different sizes of time step the following observations were made. The time step at the beginning of cooling has to be short enough for the temperature field to be accurate. The accuracy of the temperature field is most important in the glass transition range. At higher temperatures, the influence of the time step on transient stresses and residual stresses is minor. At lower temperatures when glass only has an elastic behaviour, the time step has no influence on residual stresses, though it does affect transient stresses.

6. DEFORMATIONS WITH CONSTANT LOADING

In the tempering process of flat glass, deformations are a big problem with thin glass due to roller support, which creates waviness. The waviness causes distortion of reflected light and it is a property to be avoided. With the one-dimensional quasi-static simulation program the effect of temperature on deformations for a stationary plate can be studied. The effect of support system can be also studied.

The effect of creeping is easiest to study by measuring or calculating the tip velocity at the edge of a glass plate or a cantilever beam. During secondary creeping, the tip velocity is almost constant if the glass temperature does not change. The primary creeping at the beginning is short, and it depends on the temperature. At the higher temperature the primary creeping is shorter. This is shown schematically in Fig. 6.1.

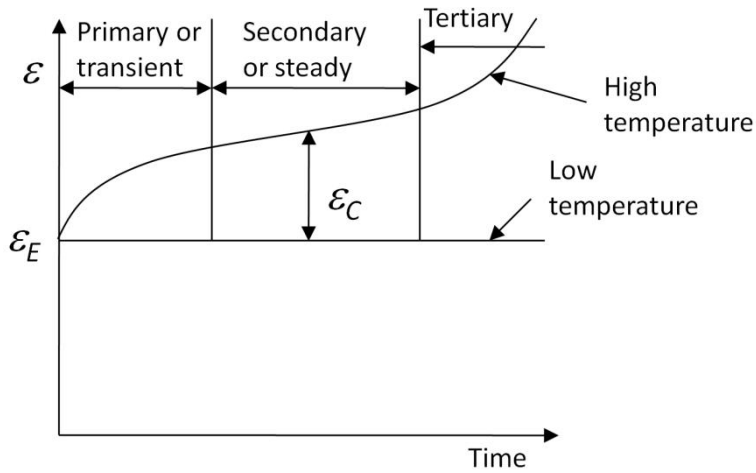

Figure 6.1. Creep behaviour under constant load (Boley & Weiner 1997).

6.1. Measurements of tip velocity

In the measurements the displacement of the edge of a narrow glass plate in Fig. 6.2 at constant temperature was measured and the tip velocity, $\dot{w}$, was calculated. The plate is fully supported along one edge and other edges are free. The measuring arrangement and support are shown in Fig. 6.3. Optical measurements were made by taking the images of the glass plate tip at a constant frequency. From the images tip velocity was calculated using Matlab®. A clear soda-lime glass with three different thicknesses (2.11 mm, 2.85 mm and 3.85 mm) and three different lengths (50 mm, 75 mm and 100 mm) was used. The width of the plate was 20 mm. The temperature range was from 550 °C to 650 °C, depending on the thickness and the plate length. Figure 6.4 presents the measured displacement as a function of time for one case. From the displacement data the velocity is calculated. In Fig. 6.5 the tip velocity of plates with different thickness or lengths is shown. In the measurements the glass temperature was raised in 10 °C steps and deformations were measured after the temperature field was stable.

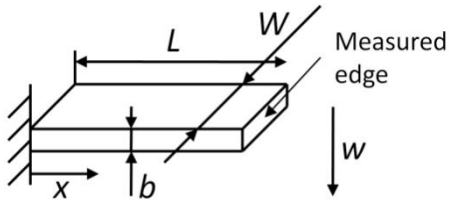

Figure 6.2. Experimental set-up of glass plate.

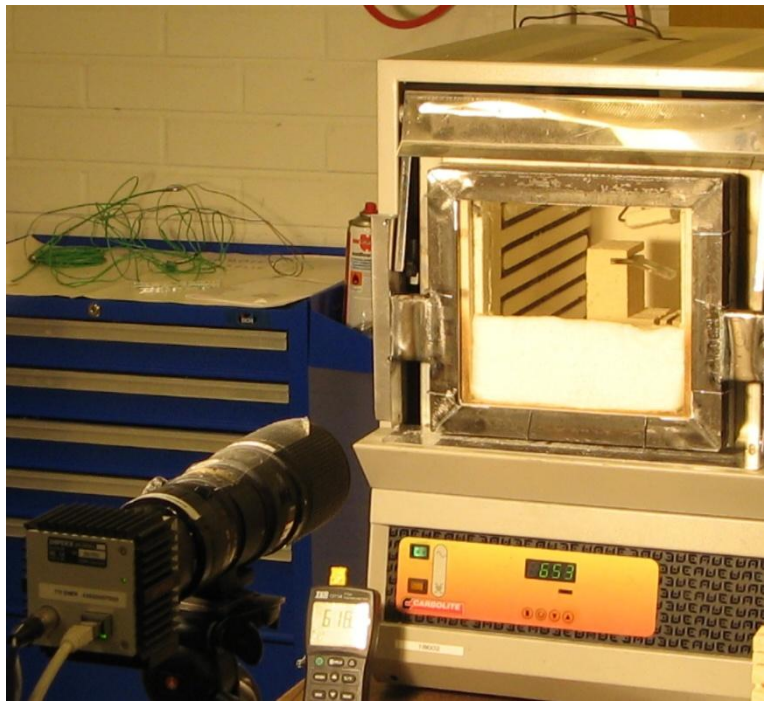

Figure 6.3. Measuring arrangement and support of the glass plate.

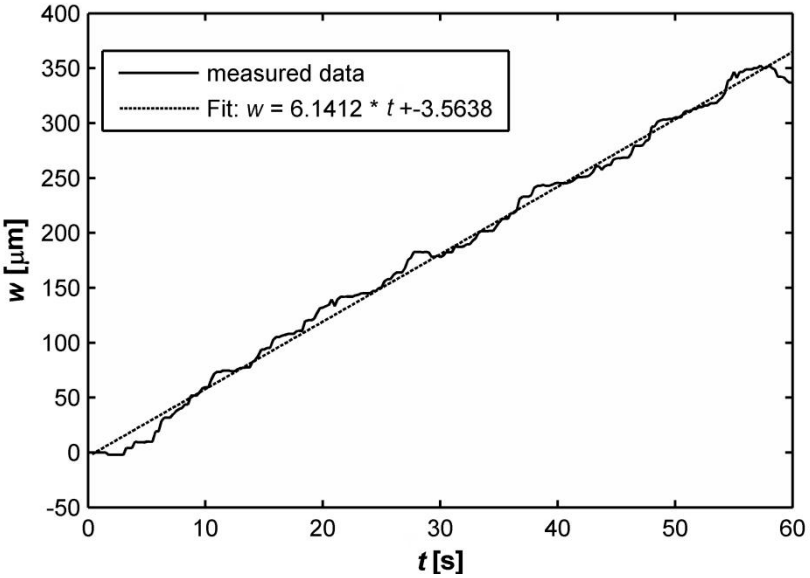

Figure 6.4. Measured displacement of plate edge as a function of time. Tip velocity is 6.192 µm/s. Thickness 2.85 mm, length 100 mm and temperature 593 °C.

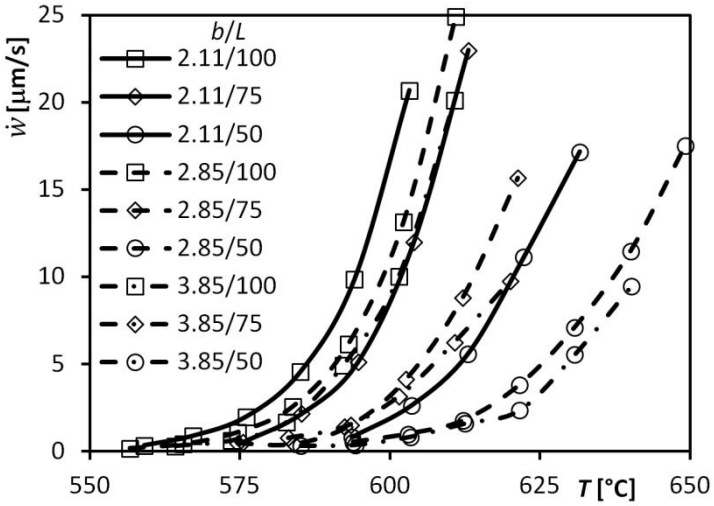

Figure 6.5. Measured tip velocity of plate.

The bending of a narrow plate in Fig. 6.2 can be compared to the bending of a cantilever beam in an elastic case. With the deflection curve *w(x)* for a cantilever beam bent by a uniform load, q_0 can present the maximum deflection of the cantilever beam w_{max}. The deflection curve in an elastic case is (Beer *et al.* 1992)

$$w(x) = \frac{q_0 L^4}{24EI}\left(\left(\frac{x}{L}\right)^4 - 4\left(\frac{x}{L}\right)^3 + 6\left(\frac{x}{L}\right)^2\right) \tag{6.1}$$

and the maximum deflection is then (Beer *et al.* 1992)

$$w_{max} = w(L) = \frac{q_0 L^4}{8EI} \tag{6.2}$$

For the narrow rectangular beam the moment of inertia I is

$$I = \frac{b^3 W}{12} \tag{6.3}$$

and the uniform load is

$$q_0 = \rho g b W \tag{6.4}$$

where g is the gravitational acceleration.

By substituting Eqs. (6.3) and (6.4) in Eq. (6.2), the maximum deflection is

$$w_{max} = \frac{3\rho g L^4}{2Eb^2} \tag{6.5}$$

The results for the measured or calculated tip velocity $\dot{w}$ can be modified using the elastic maximum deflection. The modified tip velocity is

$$\ln(\dot{w}') = \frac{\dot{w}}{w_{max}} \tag{6.6}$$

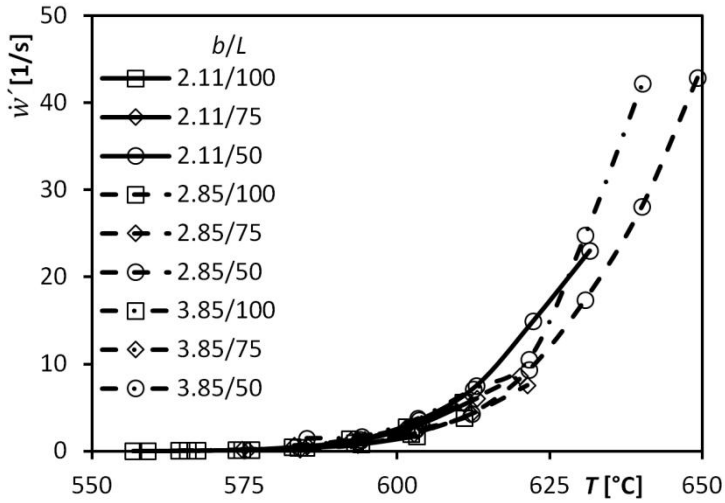

Figure 6.6. Measured values of the modified tip velocity of the plate edge.

The tip velocity depends exponentially on temperature. The Arrhenius equation (3.28) can be used to study the effect of temperature on the tip velocity. Figure 6.7 shows the relation between the tip velocity and the inverse of temperature. There are many possible sources of error in the measurements. The length of the glass plate has a major effect on the results because the creeping speed is proportional to the fourth power of the length. The tip velocity with short plates at low temperatures is slow and displacements are small and hard to measure. At high temperatures the displacement is large and the theory of small displacements cannot be used.

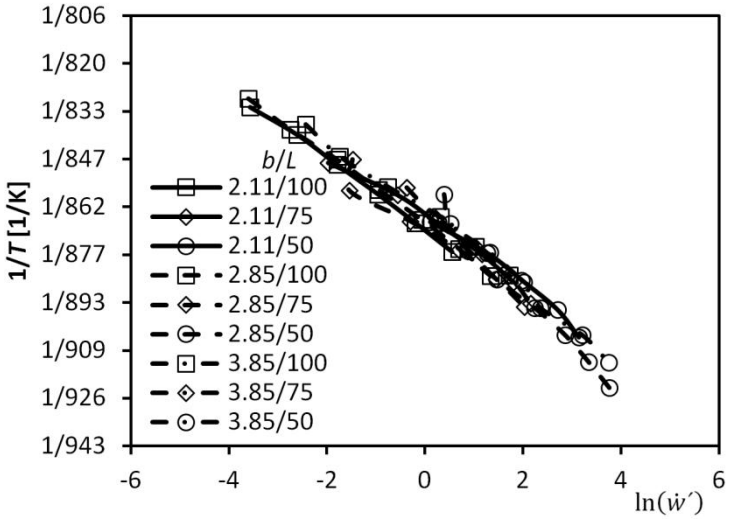

Figure 6.7. Relation between tip velocity and inverse of temperature.

According to Fig. 6.7, the lines are all almost straight and the deviation between the measured data from different beams is small. From the results it can be concluded that the Arrhenius equation (3.28) works well for glass. With the help of the measured results shown in Fig. 6.8, the activation energy, *H/R*, can be calculated

$$\ln(\dot{w}') = 66693\text{K}\left(\frac{1}{866.4\text{K}} - \frac{1}{T}\right) \tag{6.7}$$

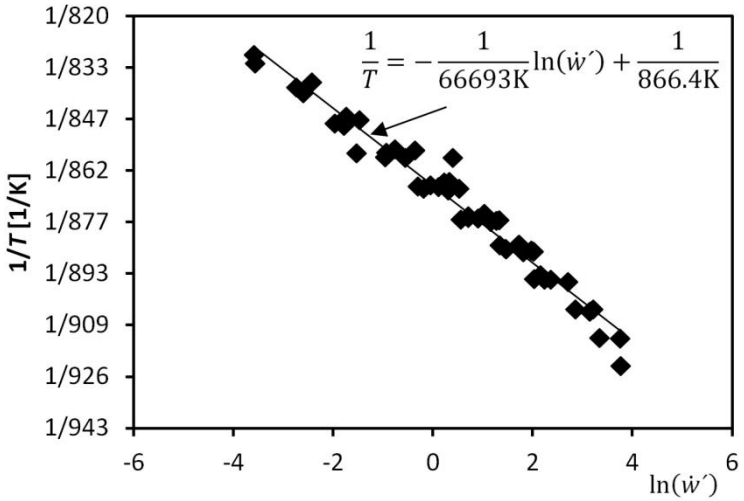

Figure 6.8. Relation between measured tip velocity and inverse of temperature with best fit line.

6.2. Calculation of tip velocity

The one-dimensional simulation program can be used to study the displacements of the plate. In the simulation program the simplifications usually needed in analytic solutions such as spatially uniform or time independent temperature fields, do not need to be taken into account.

The support and the weight of the plate are taken into account with the moment (Eq. (4.18)). In the case of the narrow glass plate shown in Fig. 6.2, the normal forces in the x and y directions are zero as is also the moment in the y direction. The moment in the x direction is

$$M_x(x) = -\frac{1}{2}\rho g b W (L - x)^2 \tag{6.8}$$

Figure 6.9 shows the simulation results using the material properties presented in Appendix A.

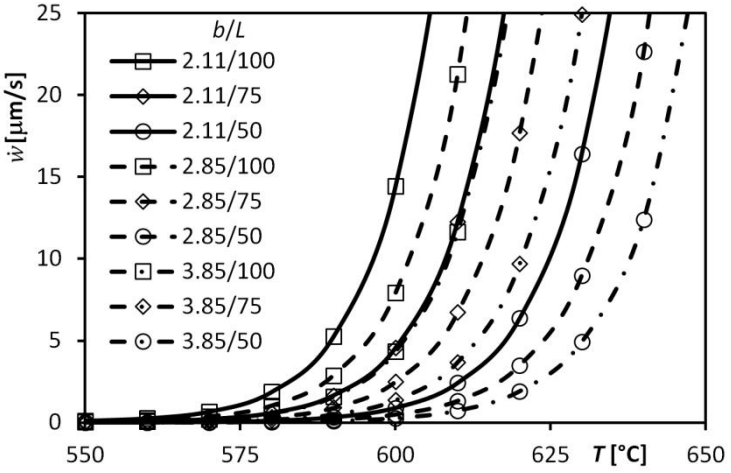

Figure 6.9. Simulation results for the tip velocity of the plate edge.

When comparing measured and calculated results in Figs. 6.5 and 6.9, the effect of temperature is seen to be different in the two cases. The same phenomenon can be seen in Fig. 6.10 where the relation between the tip velocity and the inverse of the temperature is shown. This figure presents the best fit line of the calculation results and equation for the curve and the curve from the measured results in Fig. 6.8. The accuracy of *H/R* is due to the results at low temperature. The *H/R* should be 76200 K. The activation energy, *H/R*, from the measured results is lower than from the simulated results and it illustrates the effect of temperature on tip velocity. Because the measured and calculated results are close each other the values of Appendix A, are used in following simulations and the possible changes in relaxation times between tested material and Appendix A should be discounted.

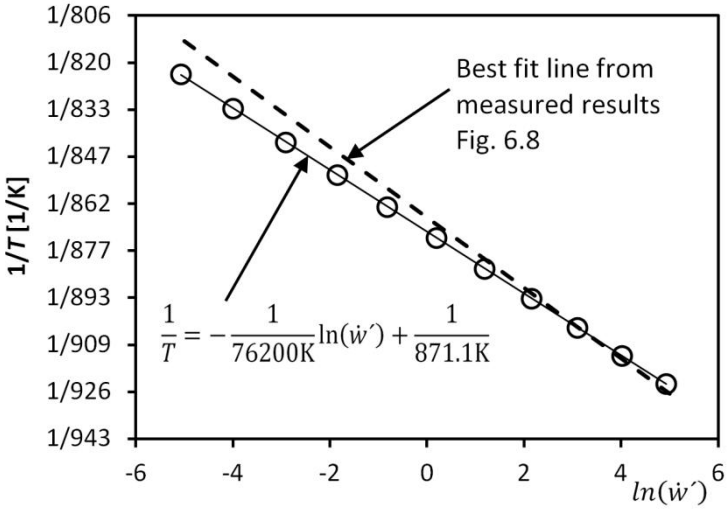

Figure 6.10. Relation between calculated tip velocity (○–○) and measured tip velocity (– – –).

6.3. Other methods

The deformations of glass can also be predicted using the correspondence principle. The principle is workable for viscoelastic beams under uniaxial stress. The method can be used for cases similar to those above.

The idea is to replace the Young's modulus E in the equation for an elastic beam with the inverse of creeping compliance. Equation (6.5) can then be modified into the form

$$w_{max}(t) = \frac{3\rho g L^4}{2b^2} J_u(t) \tag{6.9}$$

The creep compliance of glass differs from that of the stress relaxation. Because relaxation times for shear and bulk moduli are known, the three-dimensional equations are used to solve creep compliance.

The total deviatoric strain e_{ij} is the sum of the elastic e_{ij}^E and viscous e_{ij}^V deviatoric strains. For deviatoric strain, the delayed strain is zero because G_∞ is zero for glass

$$e_{ij} = e_{ij}^E + e_{ij}^V \tag{6.10}$$

Elastic and viscous deviatoric strains are

$$e_{ij}^E = \frac{s_{ij}}{2G_0} \tag{6.11}$$

$$e_{ij}^V = \frac{s_{ij} t}{2\eta} \tag{6.12}$$

Total strain for dilatation behaves similarly to that for pure shear. The total strain of dilatation $\bar{\varepsilon}$ is composed of the elastic $\bar{\varepsilon}^E$ and delayed dilatational strain $\bar{\varepsilon}^D$.

$$\bar{\varepsilon} = \bar{\varepsilon}^E + \bar{\varepsilon}^D \tag{6.13}$$

With dilatational strain viscous strain does not occur. Elastic and delayed strains of a dilatation are

$$\bar{\varepsilon}^E = \frac{\bar{\sigma}}{3K_0} \tag{6.14}$$

$$\bar{\varepsilon}^D = \bar{\sigma}\left(\frac{1}{3K_\infty} - \frac{1}{3K_0}\right)\left(1 - \sum_{i=1}^{P} w_{2i}\exp\left(-\frac{t}{\tau_{2i}}\right)\right) \tag{6.15}$$

By substituting Eqs. (6.10) – (6.15) in Eq. (3.12), the strain in direction 1 can be solved.

$$\begin{aligned}\varepsilon_{11} = e_{11} + \frac{1}{3}\bar{\varepsilon} = \frac{s_{11}}{2G_0} + \frac{s_{11}t}{2\eta} + \frac{\bar{\sigma}}{9K_0} \\ + \bar{\sigma}\left(\frac{1}{9K_\infty} - \frac{1}{9K_0}\right)\left(1 - \sum_{i=1}^{P} w_{2i}\exp\left(-\frac{t}{\tau_{2i}}\right)\right)\end{aligned} \tag{6.16}$$

from which the uniaxial stress is

$$s_{11} = \frac{2}{3}\sigma_{11} \qquad \bar{\sigma} = \sigma_{11} \tag{6.17}$$

Thus, the creep compliance for uniaxial stress is

$$J_u(t) = \frac{\varepsilon_{11}}{\sigma_{11}} = \frac{1}{E}\left[1 + \frac{t}{3\eta/E} + \left(\frac{1-2\nu}{3\,K_\infty/K_0} - \frac{1-2\nu}{3}\right)\left(1 - \sum_{i=1}^{P} w_{2i}\exp\left(-\frac{t}{\tau_{2i}}\right)\right)\right] \tag{6.18}$$

In Eq. (6.18) the term $3\eta/E$ can be expressed using the relaxation time for uniaxial stress τ_u. It can be replaced by the shear relaxation time

$$\frac{3\eta}{E} = \frac{3G_0}{E}\sum_{i=1}^{Q} w_{1i}\tau_{1i} = \frac{3}{2(1+\nu)}\sum_{i=1}^{Q} w_{1i}\tau_{1i} = \tau_u \tag{6.19}$$

The maximum deflection of a viscoelastic beam is

$$w_{max}(t) = w_{max}(0)\left[1 + \frac{t}{\tau_u} + \frac{1-2\nu}{3}\left(\frac{1}{K_\infty/K_0} - 1\right)\left(1 - \sum_{i=1}^{P} w_{2i}\exp\left(-\frac{t}{\tau_{2i}}\right)\right)\right] \tag{6.20}$$

The last term of Eq. (6.18) shows the effect of primary creeping. At high temperature the effect of the primary creeping can be neglected. The effect of temperature can be taken into account by replacing the time *t* with the reduced time ξ.

An analytical solution, Eq. (6.20), works for beams and plates with different support at the uniform temperature field. However, temperature can change during creeping. The simulation program is needed if the temperature field is non-uniform.

Fig. 6.11 shows the results of creeping from Eq. (6.20) and those of the simulation program presented in Chapter 4. During primary creeping an error develops, but the slope, i.e., creeping speed, during the secondary creeping is the same.

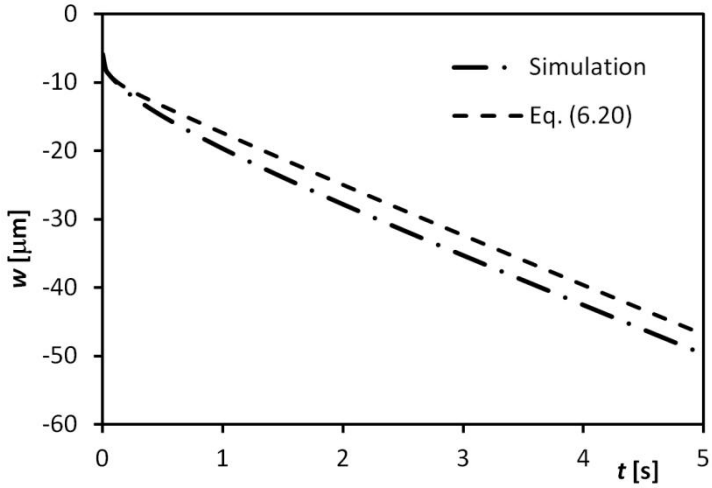

Figure 6.11. Deflection of glass plate edge in creeping. Thickness 3 mm, length 10 cm and temperature 600 °C.

From Eq. (6.20) it can be seen that the primary creeping is also proportional to the initial deflection. The duration of primary creeping depends on the temperature.

6.4. Effect of coating

The coating of glass changes the behaviour of glass plate. Tempered glass can have a low emissivity coating. One coating material is tin oxide SiO_2. The coating is very thin (100 – 1000 nm), but the different material properties of the coating material with respect to the glass can change the mechanical behaviour of the composite plate. The material properties of a thin film can be very different from those of chemically identical bulk

materials (Rouzand *et al.* 1995). A knowledge of the influence of the coating on tempered glass quality is important.

6.4.1. Measured results

In the measurements the tip velocity of Low-E glass was tested. Separate measurements were made with the coating on the top surface and on the bottom surface. In Fig. 6.12 it can be seen that the coating side adopted has an effect on the tip velocity.

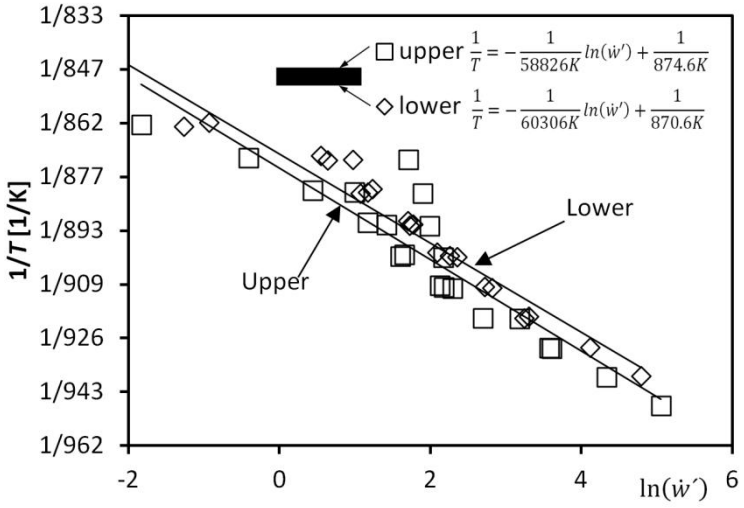

a) Glass thickness 5.85 mm

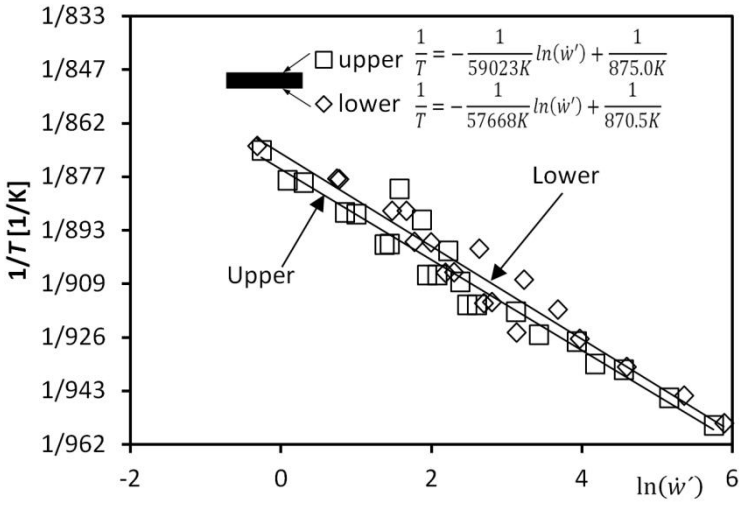

b) Glass thickness 7.85 mm

Figure 6.12. The relation between the measured tip velocity and the inverse of the temperature and the best fit line for coated glasses.

The tip velocity is faster when the coated side is downwards. One possible reason for the different behaviour is the time-dependent thermal expansion.

6.4.2. Simulation results

To study the effect of coatings, simulations were undertaken for a coated glass. In the simulations the substrate material was soda-lime glass. The coating material is tin oxide. The tin oxide film was supposed to behave elastically. The material properties for soda-lime glass and tin oxide coating are given in Appendix A.

The simulations were done with the Ansys® 13.0 Academic Research FEM program. In the simulations the total thickness of the glass is 3 mm, the length is 0.1 m and the temperature is 600 °C. The thickness of the coating is 100 nm. The simulations were performed for two cases. Figure 6.13 shows results when the glass is at a constant uniform temperature during the whole simulation. Under these conditions the coating slows down the creeping due to the non-viscous behaviour of the coating, but the side coated has no effect on the tip velocity.

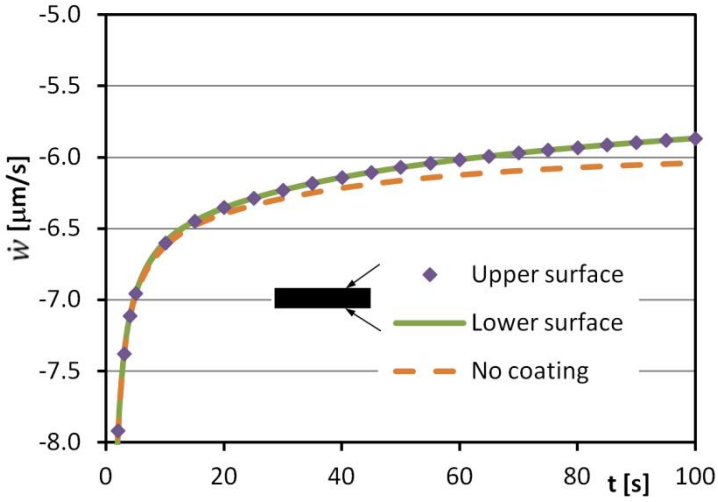

Figure 6.13. Calculated tip velocity for coated glass at constant temperature.

In the second case in Fig. 6.14, there is a temperature step change from 590 °C to 600 °C at the time 0 s. Under these conditions the effect of the time-dependent thermal expansion can be investigated. After the temperature change, the tip velocity caused by the coating was different. Results were similar compared to the measured results. It was, however, difficult to get the solution to converge due to the thickness of coating.

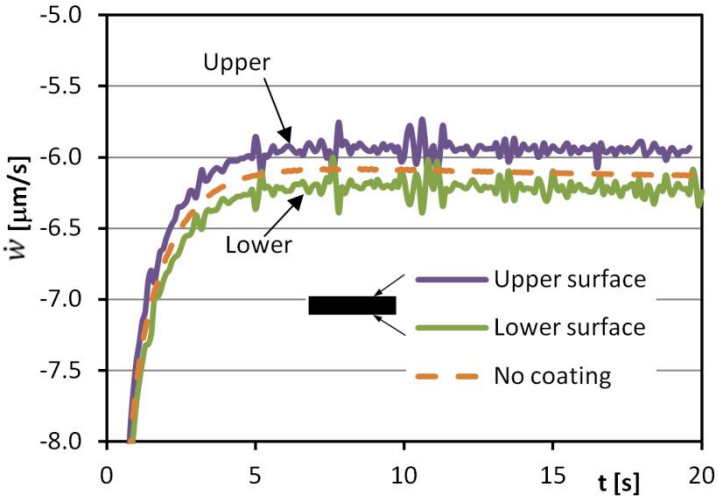

Figure 6.14. Calculated tip velocity for coated glass. Step change in temperature.

7. STRESSES AND DEFORMATIONS OF MOVING GLASS PLATE

In the case of moving glass, a three-dimensional treatment of the glass plate is needed. The movement changes the support of the rollers on the glass surface and the heat transfer can vary according to the position. This chapter examines the effect of different parameters on deformations of the glass plate and the effect of heat transfer on transient and residual stresses. For the three-dimensional simulation the ANSYS® 13.0 Academic Research program is used. In the FEM simulations the displacements are usually very small and hence certain simplifications can be made. A major problem in the calculations was how to treat the contact between the glass and rollers. When the front edge of the plate rises to a new roller, the forced displacement is presented. The plate then gains momentum making it possible for the plate to fly off the rollers. In the simulations the contact is simplified so that the upper surfaces of all the rollers in the set are in the same plane and there is no separation between the glass and any of the rollers. This simplification reduces the vibration and makes the simulation possible, otherwise it would be difficult to find a solution. Calculations were made by using an implicit solver.

7.1. Effect of parameters on deformations

At constant temperature, there are many parameters which affect the glass deformations. The change of plate thickness, velocity, temperature and roller-to-roller distance have different effects on deformations. To increase the visual quality of the glass, the effect of these parameters needs to be known.

In the simulations below the effect of the parameters on the deformations is studied with a thin glass sheet. A diagram of the rollers and the glass plate and dimensions are shown in Fig. 7.1. In the reference cases the glass thickness is 3 mm, the length is 1 m and 4 m, the distance between the rollers is 0.12 m and the glass velocity is 0.2 m/s. The temperature in the reference simulations is 630 °C. In the simulations the glass plate is very narrow with a width of 2 cm to reduce the number of elements. In the simulations time step was defined so that the displacement in the moving direction is 6.67 mm during each time step.

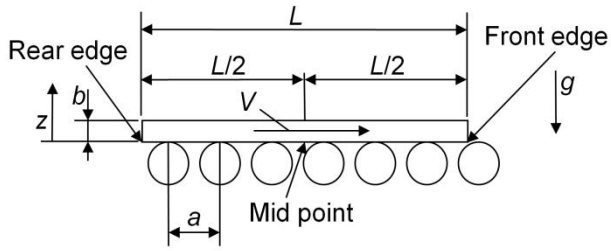

Figure 7.1. Diagram of the moving glass

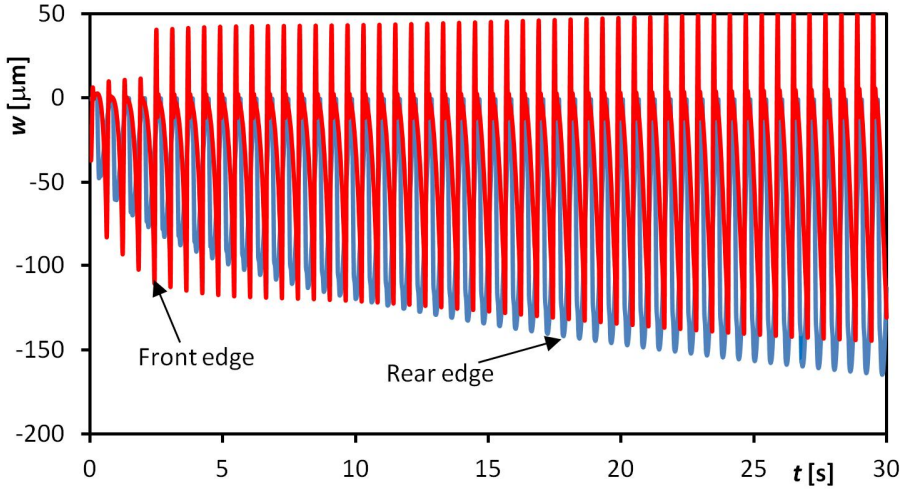

a)

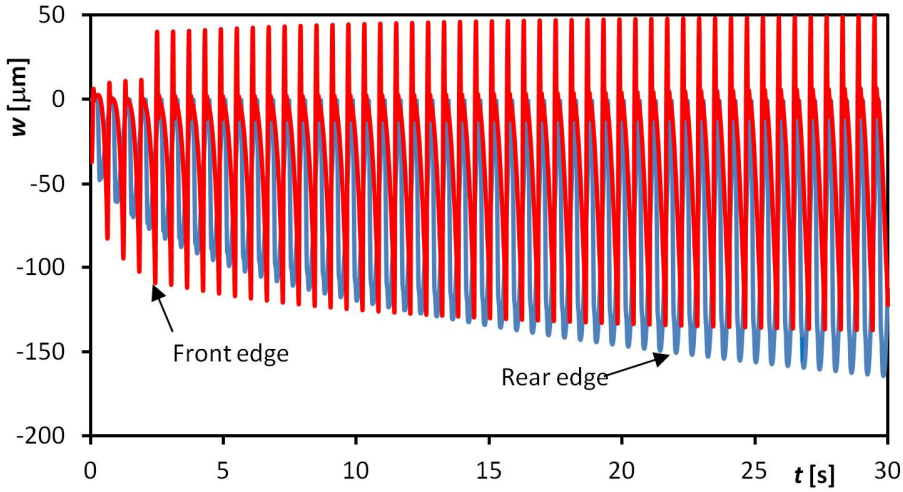

b)

Figure 7.2. Displacements of front and rear ends of reference case as a function of time. Glass length in a) 1 m and in b) 4 m.

Figure 7.2 shows the deflections of the front and rear edges of a glass plate. The length of glass is 1 m in Fig. 7.2a and 4 m in Fig. 7.2b. The behaviour of the glass edges is similar, irrespective of glass length. At the front edge the rise on the roller causes a high velocity upwards movement due to the forced displacement in the transient simulation. At the rear edge, the glass drops from the rollers and then it starts to vibrate. The vibration dampens as the distance decreases from the rear edge of the plate to the next roller. Due to the front edge rising on the roller and the rear edge dropping from the roller, the front edge is elevated above the rear edge.

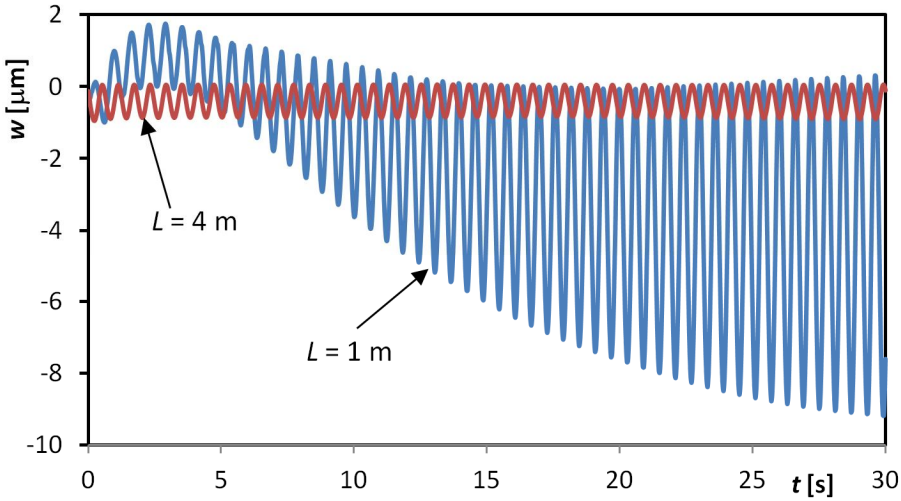

Figure 7.3. Displacements of mid-point of reference case as a function of time.

The glass ends dominate the behaviour of the entire glass plate. The deformations of glass mid-point are shown in Fig. 7.3. This figure shows the effect of the edges on the middle part of the sheet. In the case of 4 m glass plate, the distance from the edges is sufficient to reduce the effects of the ends. For comparison, at room temperature (elastic) the maximum deflection during the motion for the ends is -19 μm and for the midpoint it is -0.3 μm for both lengths. The difference for elastic displacements is due to the support of the plate. For viscoelastic material the difference is higher, as shown in Figs. 7.2 and 7.3.

The effect of the ends on centre part of the plate can also be seen in Fig. 7.4 where the deformations over the whole length are shown for 1 m (Fig. 7.4a) and 4 m (Fig. 7.4b) glass plates. In these figures the location of plates are shifted according to rollers.

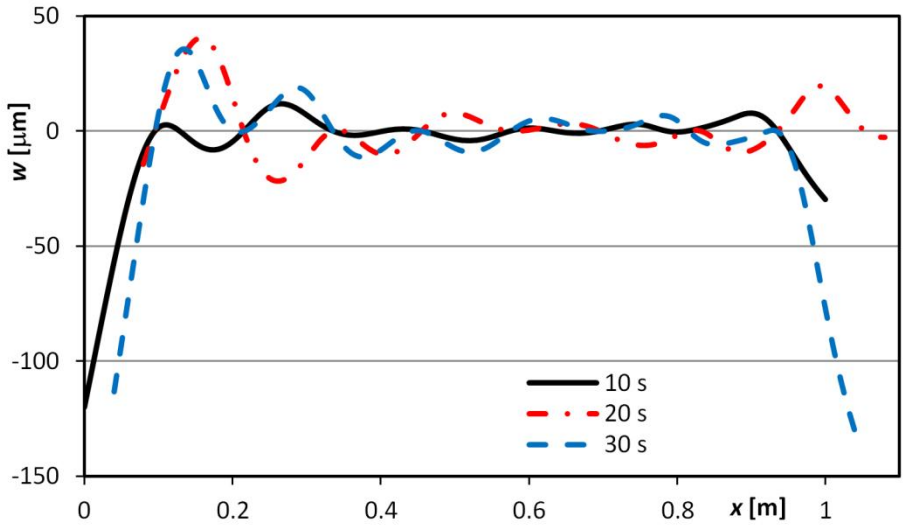

a)

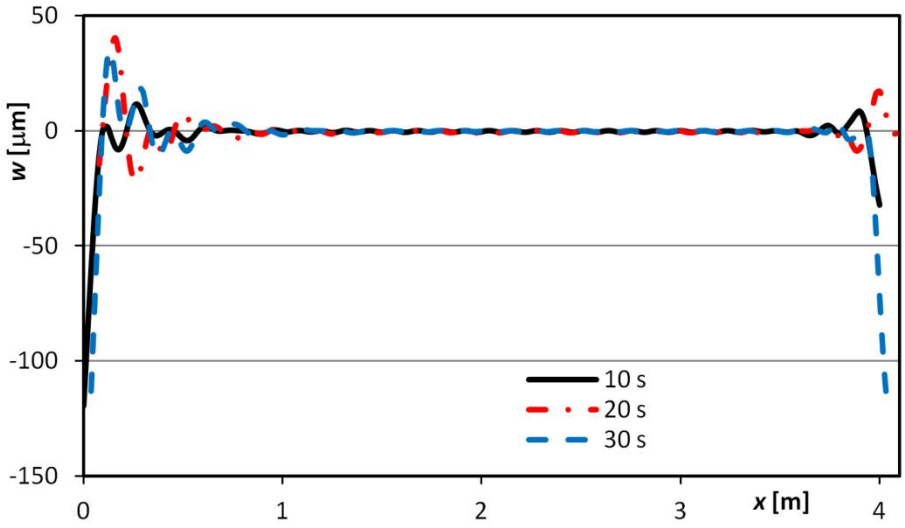

b)

Figure 7.4. Displacements of the glass plate in the reference case at different times. Glass length is 1 m (a) and 4 m (b).

7.1.1. Effect of glass thickness on deformations

As an approximation, the effect of a glass thickness is similar to the effects discussed in Chapter 6 and presented in Eqs. 6.5 and 6.6. Figure 7.5 presents the ratio of simulation results between two different thicknesses (3 mm and 4 mm) at time 30 s. The results show that the ratio is proportional to b^{-2} ($(3/4)^{-2} = 1.78$). Most of ratios are between 1.5 and 2.0. Some of the deviations result from the numerical errors during the calculations due to the small displacements.

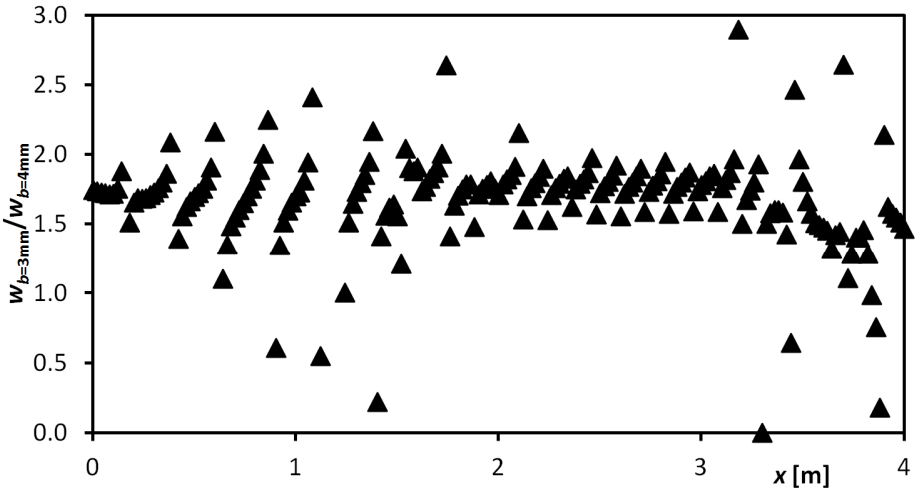

Figure 7.5. Ratio of displacements between two glass thicknesses (3 mm / 4 mm) at time 30 s.

7.1.2. Effect of roller-to-roller distance on deformations

The effect of roller-to-roller distance is more complicated. The front and rear edges dominate the deformations and when the roller-to-roller distance changes, the maximum distance from the front and rear edge to the nearest roller also changes. In Fig. 7.6 the displacement of the front end in the z-direction during the movement is shown. The deformation is much smaller with a smaller roller-to-roller distance.

The ratio of the front edge deformations for two different roller-to-roller distances differs from the results shown in Chapter 6. Figure 7.7 presents the ratio between two curves for maximum deflection at two different roller-to-roller distances (0.12 m and 0.08 m). The curves for maximum deflections are shown in Fig. 7.6. If the deformations were proportional to fourth power of the roller-to-roller distance, as shown in Eqs. 6.6. and 6.7, then the ratio would be about 5.1. The calculated ratio is larger than 5.1, but using the fourth power of the roller-to-roller distance is a good approximation of the ratio for deformations.

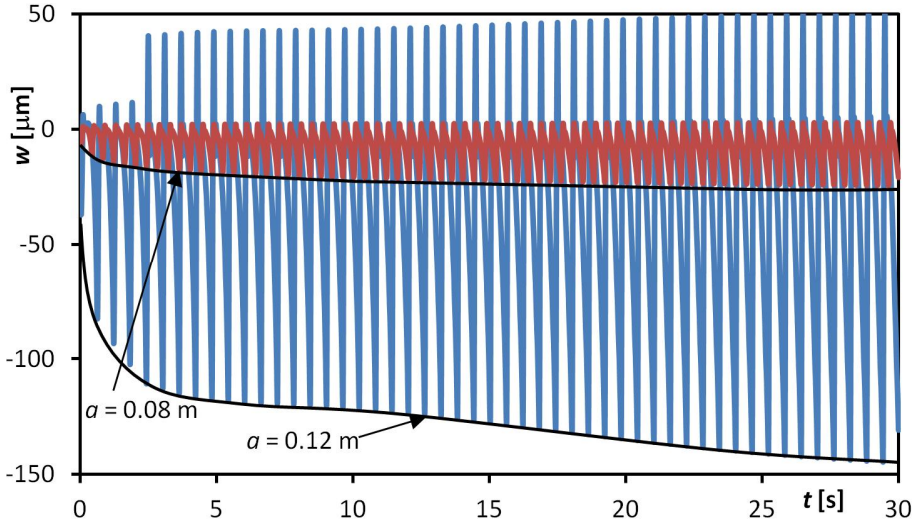

Figure 7.6. Effect of roller-to-roller distance on the front edge displacement. Glass length is 1 m.

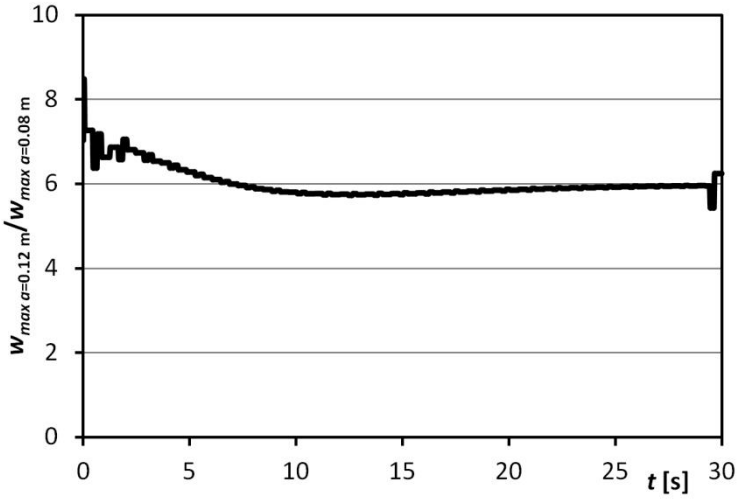

Figure 7.7. Ratio of maximum deflections from Fig 7.6 for two different roller-to-roller distances.

7.1.3. Effect of glass velocity on deformations

The glass velocity also affects the deformations. A lower velocity increases the maximum deflection, as shown in Fig. 7.8, for velocities 0.1 m/s and 0.2 m/s. If the velocity is half, the maximum deflection in the front end of the plate increases by a factor of about 1.5, as shown in Fig. 7.9. With thin glass when the deformations are greater, higher velocity is needed to reduce them. The increased velocity requires a longer tempering furnace or oscillation of the glass during heating. The effect of oscillation was not studied in the simulations.

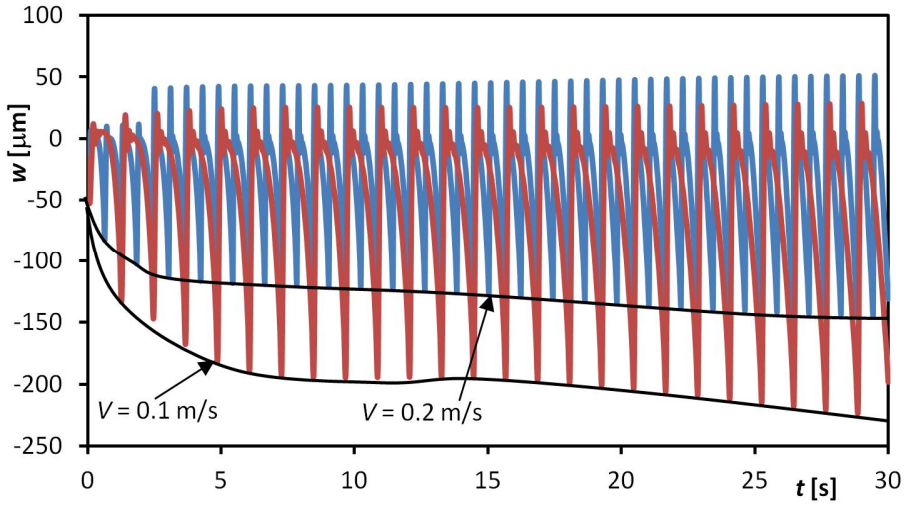

Figure 7.8. Effect of the glass velocity on front edge displacement. Glass length is 1 m.

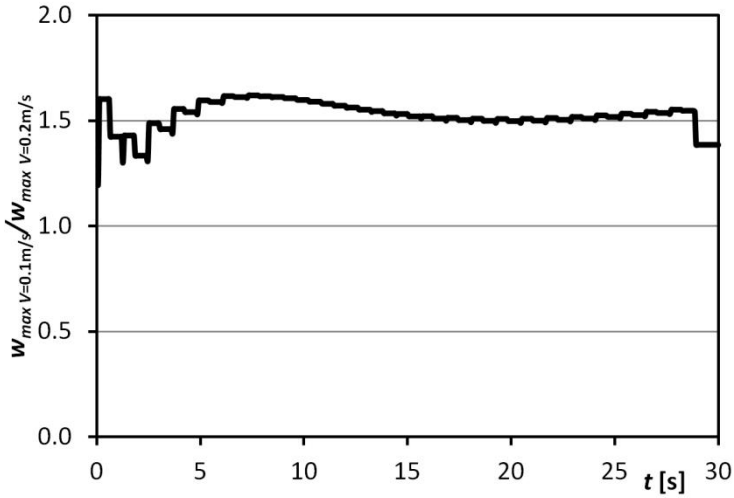

Figure 7.9. Ratio of the maximum deflections for the two different glass velocities shown in Fig. 7.8.

7.1.4. Effect of temperature on deformations

Glass deformations depend heavily on the glass temperature, especially when the temperature is above the transition temperature. In Fig. 7.10 the effect of temperature on the front end displacement is shown. The maximum displacement increases due to the temperature increase. The primary creeping at the beginning also changes due to the temperature change. After 10 seconds, the ratio between the maximum deflection curves at different temperatures is fixed to a ratio of about 1.3, as shown in Fig. 7.11. With the

ratio of shift functions at temperatures of 630 °C and 620 °C, there is a need to investigate both the ratio of deformation velocity and the deformation

$$\frac{\phi_{630℃}}{\phi_{620℃}} = \frac{exp\left(76200K\left(\frac{1}{869K} - \frac{1}{(630+273)K}\right)\right)}{exp\left(76200K\left(\frac{1}{869K} - \frac{1}{(620+273)K}\right)\right)} = 2.57 \tag{7.1}$$

From these results it is hard to predict the effect of temperature.

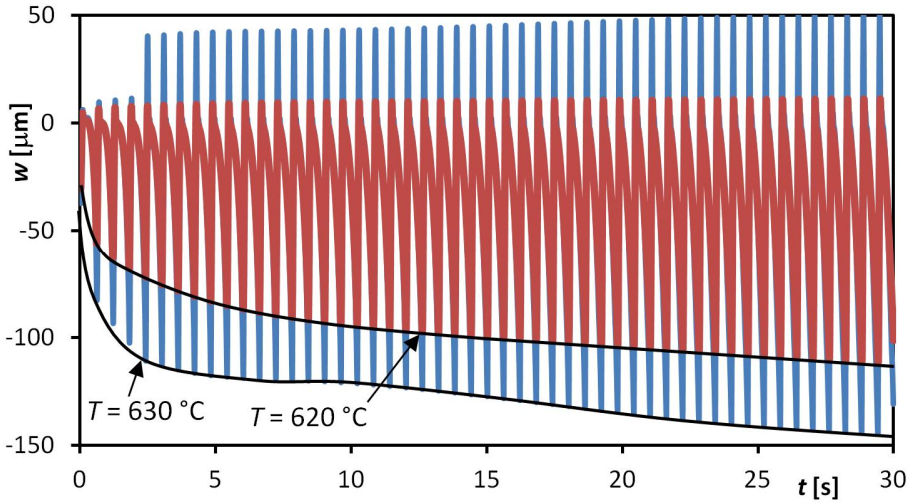

Figure 7.10. Effect of temperature on front edge displacement. Glass length is 1 m.

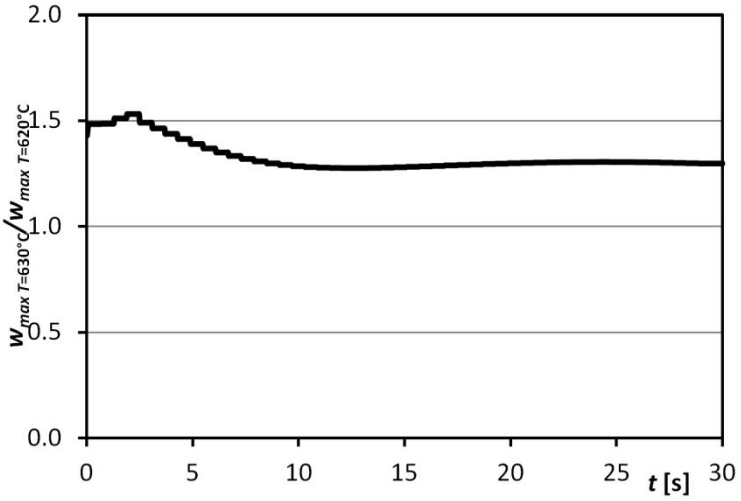

Figure 7.11. Ratio of maximum deflections at the two different glass temperatures shown in Fig. 7.10.

7.2. Effect of modified cooling

In the cooling section, forced convection is produced with pressurised air. The distance between the nozzle stagnation points is about 50 mm so that the local heat transfer coefficient varies. The glass velocity is between 100 and 800 mm/s depending on the glass thickness. With the three-dimensional FEM program, the effect of locally changing and time-dependent heat transfer coefficient on stress can be studied. In the example below, the glass thickness is 3 mm and the width and length is 0.25 m. Only the temperature field is taken into consideration and the external forces are ignored.

In order to study the effect of varying the heat transfer coefficient on stress, it has been assumed that heat transfer coefficient is

$$h(x,y,t) = h_0 + \Delta h \cdot \mathrm{abs}\left(\sin\left(\pi\frac{x-vt}{\lambda}\right) + \sin\left(\pi\frac{y}{\lambda}\right)\right) \tag{7.2}$$

where x and y are the coordinates and λ is the distance between nozzles. In the case where the glass is in the motion, the local heat transfer coefficient depends on the velocity v and time t. In Fig. 7.12 the local heat transfer coefficient distribution on the glass surface with a specific nozzle system is shown using Eq. (7.2).

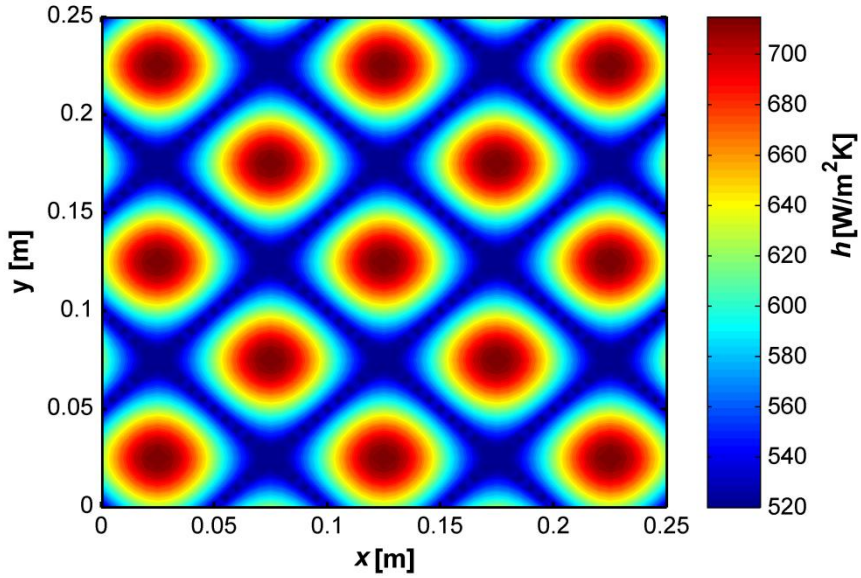

Figure 7.12. Local heat transfer coefficients. Average heat transfer coefficient is 601 W/m^{2}K, when h_0 is 520 W/m^{2}K, Δh is 100 W/m^{2}K and λ is 0.05 m.

The residual stress results for a stationary glass plate and those for a moving glass plate illustrate the reasons for the local stress differences. For the stationary case the local residual stress differences on the surface and mid-plane are shown in Figs. 7.13a and 7.13b. Fig. 7.14 shows the corresponding results when the velocity of glass in the x direction is 0.1 m/s. In these simulations the initial temperature is 650 °C. The local stress differences are greater for a stationary plate than for a plate in motion during cooling. This is another reason, in addition to that presented in Chapter 7.1.3, for high glass plate velocity.

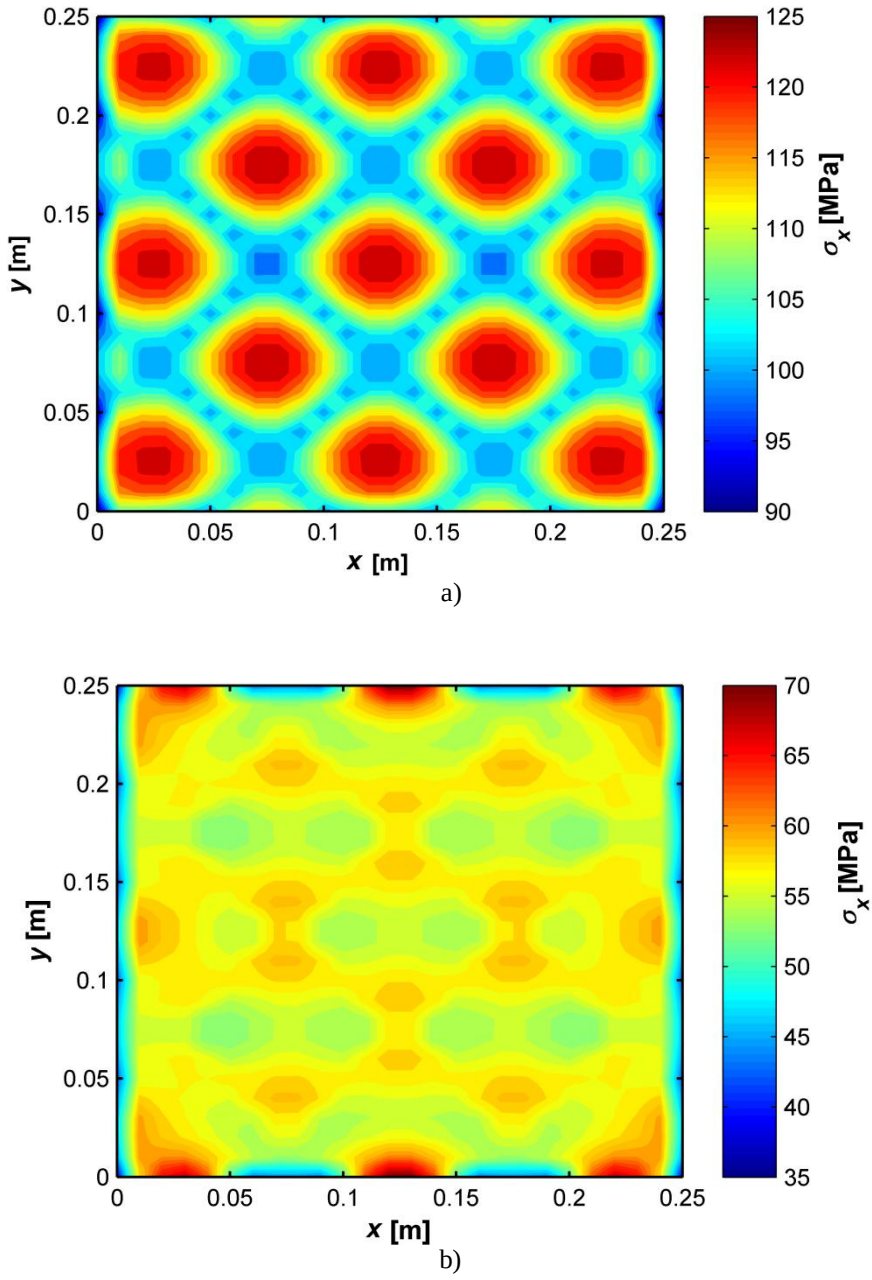

Figure 7.13. Residual stresses in x direction for stationary glass plate. (a) surface compression and (b) mid-plane tension.

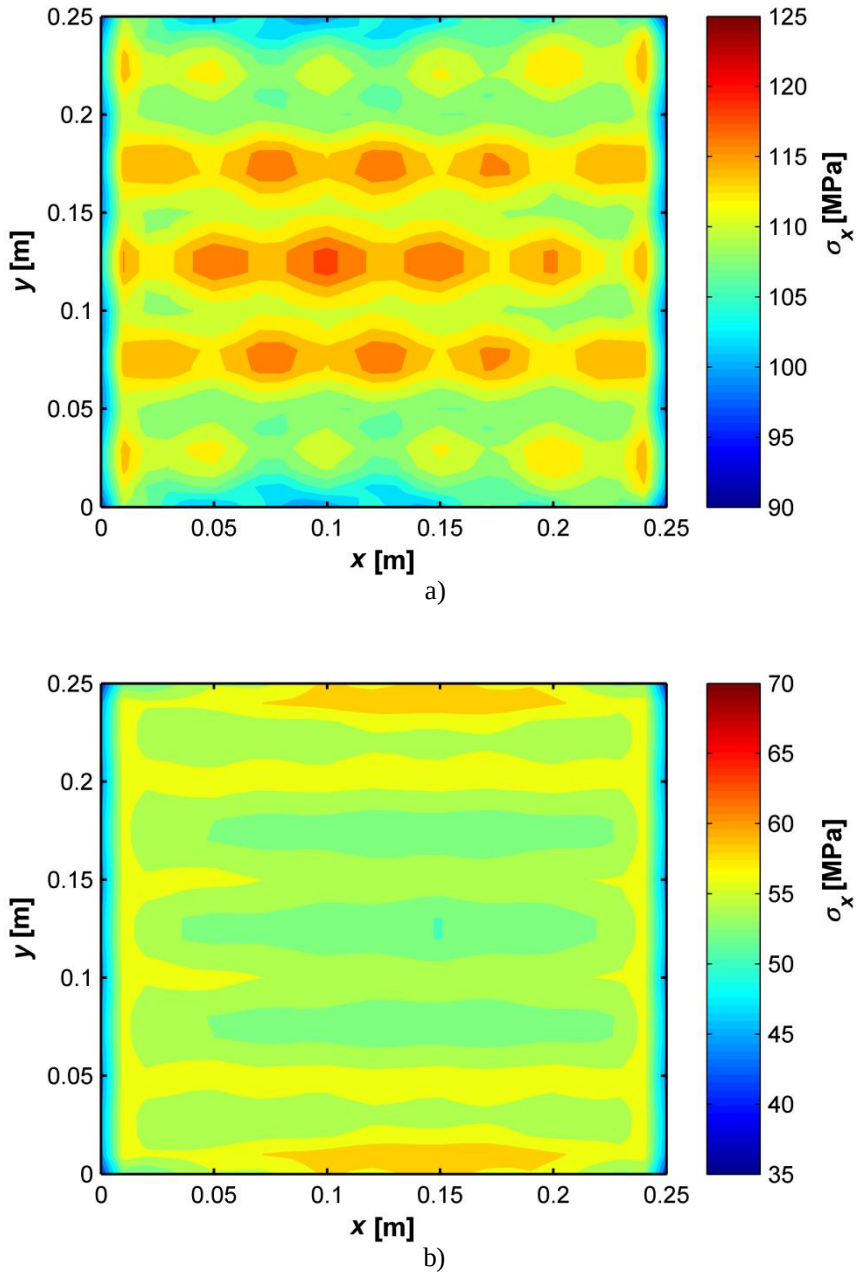

Figure 7.14. Residual stresses in x direction for moving glass plate. (a) surface compression and (b) mid-plane tension.

In the stationary plate the stress difference on the surface can be over 20 MPa whereas in the moving plate it is less than 10 MPa. For comparison, the average surface compression is 110.7 MPa and the mid-plane tension is 56.5 MPa with a constant heat transfer coefficient of 600 W/m^{2}K for the whole plate.

8. SUMMARY

The goal of the study is to find a way to improve the quality of tempered glass. The stresses and deformations during the process were investigated using a numerical simulation. The purpose of simulating a glass tempering process was to identify the causes of the typical problems which arise in the process. Typical tempering cases are simulated by changing different parameters to determine their effect on the quality of the tempered glass. State-of-the-art numerical models were used for the simulations. A cost-effective and easy-to-use one-dimensional program and the more powerful three-dimensional FEM program ANSYS® 13.0 Academic Research were used.

The results show the influence of glass initial temperature and the heat transfer coefficient on transient and residual stresses. In addition, the simulation results of deformations show the effect of time, temperature and support on the visual quality. The results provide feedback concerning the tempering of a thin glass plate. Thin glass needs higher temperatures and higher heat transfer coefficients as well as a different support system because of the higher temperature level. The numerical results were compared with the results in the literature and also with the measured deformation results obtained during this work.

The accuracy of the simulations depends on the use of appropriate material properties. In the literature the values of the material properties vary and they give some ideas about the effect of chemical composition on material properties. Thermal conductivity and viscosity have a significant influence on transient and residual stresses. Viscosity also has an important effect on deformations.

The effect of different factors on deformations is shown for a stationary and a moving glass plate. For a stationary plate the effect of parameters is easy to demonstrate using analytic equations. In the tempering process the motion of glass and the change of support are more difficult to simulate. The influence of the support structure and the tempering parameters is shown in the results. The validation of simulated deformation results by measured results is complicated, in the case of moving plates, by the influence of the thermal and mechanical history of the glass. Ideally, the whole history needs to be known.

A three-dimensional FEM program is needed in complex simulation cases. The deformations are usually very small (less than 1 mm) and the support of glass with rollers is made at contact points and these create convergence problems. The convergence was facilitated by using contacts in the simulations which do not allow for any separation. This kind of simplification is practical for a glass at a high temperature. For simple simulation cases, the one-dimensional simulation program is very effective and it can be coded for different mathematical programs.

The tempering of coated glass has been increasing. Coating changes the thermal and mechanical behaviour of a glass plate but it brings special problems to the tempering

process. In this study only the mechanical problems due to coating have been presented. The effects of radiation changes due to the use of low-E coatings have not been examined.

With the simulation it is possible to take energy consumption into account. The initial temperature, energy consumption of forced convection, and the duration of the heating and cooling all have an effect on the use of energy. The change of initial temperature can be compensated for with the heat transfer coefficient and vice versa. Furthermore modification of the cooling schedule is a way of decreasing the total energy use by decreasing the pressure with thinner glass or shortening the cooling time with thicker glass.

Although numerical methods make the simulation of stresses and deformations created in the glass tempering process possible, many problems remain. The principal problem is to find effective methods for verifying the simulation results with measurements. There are stress measurement devices on market. Some of these can measure the surface stress and some can be used to measure the stress distribution throughout the thickness of the plate but there are still weaknesses. High stress gradients, deformations and local unevenness create problems for measurement. These problems increase with a thin plate. Measurement problems are also met when measuring temperatures and deformations. Radiation and semi-transparency make temperature measurement complex and the accuracy of deformation measurement is poor because of the small scale of the deformations.

Although the study focuses on the tempering process, most of the results can also be applied to the annealing process. Most of the quality problems that arise during annealing are similar to those in tempering and are related to stresses and to deformations.

REFERENCES

Abbott M. & Madocks J., 2001, "Roller Wave Distortion - Definition, Causes and a Novel Approach to Accurate, On-line Measurement", *Proceedings of Glass Processing Days 2001*, 18-21 June 2001, Tampere, Finland, pp. 226-230.

Adams, L.H. & Williamson, E.D., 1920a, "The Annealing of Glass", *Journal of the Franklin Institute*, vol. 190, no. 5, pp. 597-631.

Adams, L.H. & Williamson, E.D., 1920b, "The Annealing of Glass", *Journal of the Franklin Institute*, vol. 190, no. 6, pp. 835-870.

Aronen, A. & Karvinen, R., 2011, "Modeling of Deformations and Stresses during Glass Tempering", *Proceedings of the ASME 2011 International Mechanical Congress & Exposition IMECE 2011*, November 2011, Denver, Colorado, USA.

ASTM C1048-97b:1997, 1997, *Standard Specification for Heat Treated Flat Glass – Kind HS, Kind FT Coated and Uncoated Glass*, ASTM.

Bartenev, G.M., 1948, "Theory of Mechanical Strengthening of Glass by Quenching", *Doklady Akademii Nauk SSSR*, vol. 18, no. 3, pp. 383-388.

Bartholomew, R.F. & Garfinkel, H.M., 1980, "Chemical Strengthening of Glass", *in Glass Science and Technology* vol. 5 Elasticity and Strength in Glasses, D.R. Uhlmann and N.J. Kreidl (eds.), Academic Press, New York, pp. 217-270.

Beer, F.B., Johnston, E.R. & DeWolf, J.T., 2004, *Mechanics of Materials*, 2nd ed., McGraw-Hill, New York, USA.

Bejan, A., 1993, *Heat Transfer*, John Wiley & Sons, Inc., USA.

Boley, B. & Weiner, J., 1997, *Theory of Thermal Stresses*, Dover, Mineola (NY), USA.

Carré, H. & Daudeville, L., 1996, "Numerical Simulation of Soda-Lime Silicate Glass Tempering", *Journal de Physique IV*, vol. 6, no. 1, pp. 175-185.

Carré, H. & Daudeville, L., 1999, "Load-Bearing Capacity of Tempered Structural Glass", *Journal of Engineering Mechanics*, vol. 125, no. 8, pp. 914-921.

Chambers, R., 1992, "Numerical Integration of the Hereditary Integrals in a Viscoelastic Model for Glass", *Journal of American Ceramic Society*, vol. 75, no. 8, pp. 2213-2218.

Christensen, R.M., 1982, *Theory of Viscoelasticity*, 2nd ed. Academic Press, New York, USA.

Daudeville, L. & Carré, H., 1998, "Thermal Tempering Simulation of Glass Plates: Inner and Edge Residual Stresses", *Journal of Thermal Stresses*, vol. 21, no. 6, pp. 667-689.

Daudeville, L., Bernard, F. & Gy, R., 2002, "Residual Stresses Near Holes in Tempered Glass Plates", *Materials Science Forum*, vol. 404-407, pp. 43-48.

EN 12150-1:2000, 2000, *Glass in Building – Thermally Toughened Soda Lime Silicate Safety Glass – Part 1: Definition and Description*, CEN.

EN 572-1:2004, 2004, *Glass in Building – Basic Soda Lime Silicate Glass Products – Part 1:Definitions and General Physical and Mechanical Properties*, CEN.

Field, R.E. & Viskanta, R., 1990, "Measurement and Prediction of the Dynamic Temperature Distributions in Soda-Lime Glass Plates", *Journal of the American Ceramic Society*, vol. 73, no. 7, pp. 2047-2053.

Flügge, W., 1975, *Viscoelasticity*, 2nd ed., Springer-Verlag, Berlin, Germany.

Gardon, R., 1958, "Calculation of Temperature Distributions in Glass Plates Undergoing Heat-Treatment", *Journal of the American Ceramic Society*, vol. 41, no. 6, pp. 200-209.

Gardon, R., 1965, "The Tempering of Flat Glass by Forced Convection", *Proceedings VIIth International Congress on Glass*, Bryssel, Belgium.

Gardon R., 1980, "Thermal Tempering of Glass", *in Glass Science and Technology* vol. 5 Elasticity and Strength in Glasses, D.R. Uhlmann and N.J. Kreidl (Eds.), Academic Press, New York, pp. 145-216.

Gardon, R., 1988, "Tempering Glass with Modulated Cooling Schedules", *Journal of the American Ceramic Society*, vol. 71, no. 10, pp. 876-878.

Gladysz, G.M. & Chawla, K.K., 2001, "Coefficients of Thermal Expansion of Some Laminated Ceramic Composites", *Composites: Part A: Applied Science and Manufacturing*, vol. 32, no. 2, pp. 173-178.

Guillemet, C., 1990, "Annealing and Tempering of Glass", *Journal of Non-Crystalline Solids*, vol. 123, no. 1-3, pp. 415-426.

Henriksen, T. & Leosson, K., 2009, "Anisotropy and Optical Distortion in Architectural Glass, Can It Be Controlled", *Proceedings of Glass Performance Days 2009*, June 2009, Tampere, Finland, pp. 834-839.

Holger, M., 1977, "Heat and Mass Transfer between Impinging Gas Jets and Solid Surfaces", *Advances in Heat Transfer*, vol. 13, pp. 1-60.

Huber, A.M. & Viskanta, R., 1994, "Effect of Jet-Jet Spacing on Convective Heat Transfer to Confined, Impinging Arrays of Axisymmetrical Air Jets", *International Journal of Heat and Mass Transfer*, vol. 37, no. 18, pp. 2859-2869.

Indenbom, V.L., 1954, "On the Theory of Glass Hardening", *Zhurnal Tekhnicheskoi Fiziki*, vol. 24, pp. 925-928.

Karlsson, S., Jonson, B. & Stålhandske, C., 2010, "The Technology of Chemical Glass Strengthening - A Review", *European Journal of Glass Science and Technology Part A*, vol. 51, no. 2, pp. 41-54.

Kong, J., Kim, J. H. & Chung, K. 2007, "Residual Stress Analysis with Improved Numerical Methods for Tempered Plate Glasses Based on Structural Relaxation Model", *Metals and Materials International*, vol. 13, no. 1, pp. 67-75.

Kurkjian, C.R., 1963, "Relaxation of Torsional Stress in the Tranformation Range of a Soda-Lime-Silica Glass", *Physics and Chemistry of Glasses*, vol. 4, no. 4, pp. 128-136.

Le Bourhis, E., 2008, *Glass: Mechanics and Technology*, Wiley-VCH Verlag GmbH & Co, Weinheim, Germany

Lee, E.H., Rogers, T.H. & Woo, T.C., 1965, "Residual Stresses in a Glass Plate Cooled Symmetrically from Both Surfaces", *Journal of the American Ceramic Society*, vol. 48, no. 9, pp. 480-487.

Maniatis, I., 2005, *Numerical and Experimental Investigations on the Stress Distribution of Bolted Glass Connections under In-Plane Loads*, PhD Thesis, TU München, Germany.

Markovsky, A., Soules, T. & Boyd, D.C., 1984, "An Efficient and Stable Algorithm for Calculating Fictive Temperature", *Journal of American Ceramic Society*, vol. 67, no. 4, pp. C56-C57.

Mills, A.F., 1999, *Basic Heat and Mass Transfer*, 2nd ed., Prentice Hall, Inc., USA.

Modest, M.F., 1993, *Radiative Heat Transfer*, McGraw-Hill, USA.

Narayanaswamy, O. S., 1978, "Stress and Structural Relaxation in Tempering Glass", *Journal of the American Ceramic Society*, vol. 61, no. 3-4, pp. 146-152.

Narayanaswamy, O. S., 2001, "Evolution of Glass Tempering Models", *Proceedings of Glass Processing Days 2001*, 18-21 June 2001, Tampere, Finland, pp. 83-86.

Nielsen, J.H., 2009, *Tempered Glass – Bolted Connections and Related Problems*, Ph.D. thesis, DTU Civil Engineering, Lyngby, Denmark.

Nielsen, J.H., Olesen, J.F., Poulsen, P. N. & Stang H., 2010a, "Simulation of Residual Stresses at Holes in Tempered Glass: A Parametric Study", *Materials and Structures*, vol. 43, no. 7, pp. 947-961.

Nielsen, J.H., Olesen, J.F., Poulsen, P. N. & Stang H., 2010b, "Finite Element Implementation of a Glass Tempering Model in Three Dimensions", *Computers and Structures*, vol. 88, no. 17-18, pp. 963-972.

Noda, N., Hetnarski, R.B. & Tanigawa, Y., 2003, *Thermal Stresses*, 2nd ed., Taylor & Francis, New York, USA.

Rantala, M. & Karvinen, R., 2001, "Treatment of Transient Radiative Heat Transfer in Glass Tempering Prosess", *International Symposium on Radiative Transfer III*, 17-22 June 2001, Antalya, Turkey, pp. 23-25.

Rouzaud, A., Barbier, E., Ernoult, J. & Quesnel, E, 1995, "A Method for Elastic Modulus Measurements of Magnetorn Sputtered Thin Films Dedicated to Mechanical Applications", *Thin Solid Films*, vol. 270, pp. 270-274.

Scherer, G.W. & Rekhson, S.M., 1982, "Model of Structural Relaxation in Glass with Variable Coefficients", *Journal of the American Ceramic Society*, vol. 65, no. 6, pp. C94-C96.

Scherer, G., 1986, *Relaxation in Glass and Composites*, John Wiley & Sons, Inc., USA.

Schneider, J., 2004, "Glass Strength in the Borehole Area of Annealed Float Glass and Tempered Float Glass", *International Journal of Forming Processes*, vol. 7, no. 4, pp. 523-541.

Shelby, J.E., 2005, *Introduction to Glass Science and Technology*, 2nd ed., The Royal Society of Chemistry, Cambridge, UK.

Shen, W, Tang, C.Y., Li, W. & Peng, L.H., 2001, "Determining Young's Modulus of Conductive Thin Films by a Thermal Bend Beam Test", *The Journal of Strain Analysis for Engineering Design*, vol. 36, no. 2, pp. 163-168.

Siegel, R. & Howell, J., 2001, *Thermal Radiation Heat Transfer*, 4th ed., Taylor & Francis, USA.

Tool, A.Q., 1946, "Relation between Inelastic Deformability and Thermal Expansion of Glass in its Annealing Range", *Journal of the American Ceramic Society*, vol. 29, no. 9, pp. 240-253.

Zuckerman, N. & Lior, N., 2006, "Jet Impingement Heat Transfer: Physics, Correlations, and Numerical Modeling", *Advances in Heat Transfer*, vol. 39, pp. 565-631.

APPENDIX A

Material properties for soda-lime-silica glass

Table A.1. Material properties (Carré & Daudeville 1996, 1999, Daudeville *et al.* 2002)

Young's modulus E = 70 GPa
Poisson ratio ν = 0.22
Thermal expansion coefficient for solid glass $\alpha_g = 9 \cdot 10^{-6}$ 1/K
Thermal expansion coefficient for liquid glass $\alpha_l = 32 \cdot 10^{-6}$ 1/K
Thermal conductivity $k = 0.975 + 8.58 \cdot 10^{-4}$ T W/mK ,where T in °C
Specific heat of solid glass $c_{p,g}$ = 893 + 0.4 T J/kgK ,where T in K
Specific heat of liquid glass $c_{p,l}$ = 1433 J/kgK
Ratio H/R = 76200 K
Constant x = 0.5
Density ρ = 2530 kg/m^3
Environment temperature T_∞ = 20 °C

Table A.2. Characteristics of shear and bulk relaxation times and response function for structural relaxation (T_{ref} = 869 K) (Carré & Daudeville 1999)

Shear relaxation times		Bulk relaxation times (K_∞/K_0 = 0.18)		Structural relaxation	
w_{1i}	τ_{1i}	w_{2i}	τ_{2i}	C_i	λ_i
0.05523	$6.658 \cdot 10^{-5}$	0.0222	$5.009 \cdot 10^{-5}$	0.05523	$5.965 \cdot 10^{-5}$
0.08205	$1.197 \cdot 10^{-3}$	0.0224	$9.945 \cdot 10^{-4}$	0.08205	$1.077 \cdot 10^{-2}$
0.1215	$1.514 \cdot 10^{-2}$	0.0286	$2.022 \cdot 10^{-3}$	0.1215	0.1362
0.2286	0.1672	0.2137	$1.925 \cdot 10^{-2}$	0.2286	1.505
0.2860	0.7497	0.394	0.1199	0.2860	6.747
0.2265	3.292	0.3191	2.033	0.2265	29.63

Table A.3. Radiative properties of glass (Gardon 1958)

Mean reflectivity ρ_m = 0.04
Mean propagation angle α_m = 0°

Mean absorption coefficients for different wave length ranges

λ_i / μm	λ_j / μm	$a(\Delta\lambda)$ / cm^{-1}
0	2,75	0,3
2,75	4,3	4,5
4,3	∞	100

Material properties for tin oxide (SnO_2) coating

Table A.4. Material properties (Shen *et al*. 2001, Gladysz & Chawla 2001)

Young's modulus E = 164 GPa
Poisson ratio ν = 0.293
Thermal expansion coefficient $\alpha = 10.1 \cdot 10^{-6}$ 1/K
Density ρ = 6900 kg/m^3
Thickness of coating film c = 100 nm

APPENDIX B

Calculation of one dimensional case

Temperature field $T(z)$ is symmetric and bending moments $M_x = M_y = 0$. Stresses and strains in the x and y directions are equal ($\sigma_{xx} = \sigma_{yy}$, $\varepsilon_{xx} = \varepsilon_{yy}$). In calculations the equations in Chapter 4 take simpler forms as follows.

At the beginning of cooling stresses and strains are zero

$$s_{xx}^{q}(0, z_i) = \bar{\sigma}^{p}(0, z_i) = 0 \tag{B.1}$$

$$e_{xx}(0, z_i) = \bar{\varepsilon}(0, z_i) = 0 \tag{B.2}$$

where superscripts q and p represent the index of summation.

Due to the plane stress assumption also

$$\sigma_{zz}(t_n, z_i) = 0 \tag{B.3}$$

The stress field must fulfil the equilibrium equation

$$\sum_{i=1}^{Nn} \sigma_{xx}(t_n, z_i)\, \Delta z_i = 0 \tag{B.4}$$

In which

$$\sigma_{xx}(t_n, z_i) = \frac{1}{3}\bar{\sigma}(t_n, z_i)\delta_{ij} + s_{xx}(t_n, z_i) \tag{B.5}$$

where

$$\bar{\sigma}(t_n, z_i) = \sum_{p=1}^{P} \bar{\sigma}^{p}(t_n, z_i) + 3K_{\infty}[\bar{\varepsilon}(t_n, z_i) - 3\varepsilon^{th}(t_n, z_i)] \tag{B.6}$$

$$s_{xx}(t_n, z_i) = \sum_{q=1}^{Q} s_{xx}^{q}(t_n, z_i) \tag{B.7}$$

$$\begin{aligned} \bar{\sigma}^{p}(t_n, z_i) &= exp\left\{-\frac{\Delta\xi_n}{\tau_{2p}}\right\}\bar{\sigma}^{p}(t_{n-1}, z_i) \\ &+(3K_0 - 3K_{\infty})w_{2p}k_p(\Delta t_n, z_i)\{[\bar{\varepsilon}(t_n, z_i) - \bar{\varepsilon}(t_{n-1}, z_i)] \\ &\quad - [3\varepsilon^{th}(t_n, z_i) - 3\varepsilon^{th}(t_{n-1}, z_i)]\} \end{aligned} \tag{B.8}$$

$$s_{xx}^{q}(t_n,z_i) = exp\left\{-\frac{\Delta\xi_n}{\tau_{1q}}\right\}s_{xx}^{q}(t_{n-1},z_i) + 2G_0 w_{1q} g_q(\Delta t_n,z_i)\left\{[\varepsilon_{xx}^{0}(t_n)-\varepsilon_{xx}^{0}(t_{n-1})] - \frac{\delta_{ij}}{3}[\bar{\varepsilon}(t_n,z_i)-\bar{\varepsilon}(t_{n-1},z_i)]\right\} \quad (B.9)$$

In Eqs. (B.8) and (B.9) functions $k_p(\Delta t_n,z_i)$ and $g_q(\Delta t_n,z_i)$ are

$$k_p(\Delta t_n) = \frac{\tau_{2p}}{\Delta\xi_n}\left\{1 - exp\frac{-\Delta\xi_n}{\tau_{2p}}\right\} \quad (B.10)$$

$$g_q(\Delta t_n) = \frac{\tau_{1q}}{\Delta\xi_n}\left\{1 - exp\frac{-\Delta\xi_n}{\tau_{1q}}\right\} \quad (B.11)$$

The strain in the z direction is needed, because $\bar{\varepsilon}(t_n,z_i) = \varepsilon_{xx}(t_n,z_i) + \varepsilon_{yy}(t_n,z_i) + \varepsilon_{zz}(t_n,z_i)$

$$\sigma_{zz}(t_n,z_i) = \frac{1}{3}\bar{\sigma}(t_n,z_i)\delta_{ij} + s_{zz}(t_n,z_i) = 0 \quad (B.12)$$

where

$$\bar{\sigma}(t_n,z_i) = \sum_{p=1}^{P}\bar{\sigma}^{p}(t_n,z_i) + 3K_\infty[\bar{\varepsilon}(t_n,z_i) - 3\varepsilon^{th}(t_n,z_i)] \quad (B.13)$$

$$s_{zz}(t_n,z_i) = \sum_{q=1}^{Q} s_{zz}^{q}(t_n,z_i) \quad (B.14)$$

$$\bar{\sigma}^{p}(t_n,z_i) = exp\left\{-\frac{\Delta\xi_n}{\tau_{2p}}\right\}\bar{\sigma}^{p}(t_{n-1},z_i) + (3K_0 - 3K_\infty)w_{2p}k_p(\Delta t_n,z_i)\{[\bar{\varepsilon}(t_n,z_i) - \bar{\varepsilon}(t_{n-1},z_i)] - [3\varepsilon^{th}(t_n,z_i) - 3\varepsilon^{th}(t_{n-1},z_i)]\} \quad (B.15)$$

$$s_{zz}^{q}(t_n,z_i) = exp\left\{-\frac{\Delta\xi_n}{\tau_{1q}}\right\}s_{zz}^{q}(t_{n-1},z_i) + 2G_0 w_{1q} g_q(\Delta t_n,z_i)\left\{[\varepsilon_{zz}(t_n,z_i) - \varepsilon_{zz}(t_{n-1},z_i)] - \frac{\delta_{ij}}{3}[\bar{\varepsilon}(t_n,z_i)-\bar{\varepsilon}(t_{n-1},z_i)]\right\} \quad (B.16)$$

From equations above strains ε_{xx}^{0} and ε_{zz} are solved iteratively.

Tampereen teknillinen yliopisto
PL 527
33101 Tampere

Tampere University of Technology
P.O.B. 527
FI-33101 Tampere, Finland

ISBN 978-952-15-2799-9
ISSN 1459-2045